

Joint Optimization of Large and Small Models for Surface Temperature and Emissivity Retrieval Using Knowledge Distillation

Wang Dai ^{a,*}, Kebiao Mao ^{b,*}, Zhonghua Guo ^a, Zhihao Qin ^b, Jiancheng Shi ^c, Sayed M. Bateni ^d, Liurui Xiao ^a
a School of Electrical and Electronic-Engineering, Ningxia University, Yinchuan 750021, China

b State Key Laboratory of Efficient Utilization of Arid and Semi-arid Arable Land in Northern China, Institute of Agricultural Resources and Regional Planning, Chinese Academy of Agricultural Sciences, Beijing 100081, China. qinzhihao@caas.cn

c National Space Science Center, Chinese Academy of Sciences, Beijing 100190, China. shijiancheng@nssc.ac.cn

d Department of Civil and Environmental Engineering and Water Resources Research Center, University of Hawaii at Manoa, Honolulu, HI 96822, USA. smbateni@hawaii.edu

Correspondence to: Kebiao Mao (maokebiao@caas.cn).

★ These authors contributed equally to this work.

Preprint Declaration:

This preprint was originally posted on EarthArXiv prior to peer review. A revised version of this manuscript has now been accepted for publication in Artificial Intelligence in Agriculture after undergoing full peer review. The content matches the version submitted to the journal.

Declaration:

The authors declare that they have no known competing financial interests or personal relationships that could have appeared to influence the work reported in this paper.

Funding:

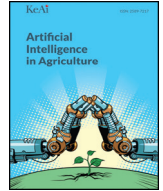
This research was supported by key Project of Natural Science Foundation of Ningxia Department of Science and Technology (No. 2024AC02032), Fengyun Satellite Application Pilot Program "Development and Application of Fengyun all-weather Land Surface Temperature Spatiotemporal Fusion Dataset" (FY-APP-2022.0205).

Acknowledgments:

We are especially thankful to NASA and Japan's Ministry of Economy, Trade and Industry (METI) for providing the ASTER thermal infrared data that were crucial for our analysis. Additionally, we are thankful to the Chinese Academy of Sciences, Institute of Geographic Sciences and Natural Resources Research for providing ground observation data.

Citation:

Wang Dai, Kebiao Mao, Zhonghua Guo, Zhihao Qin, Jiancheng Shi, Sayed M. Bateni & Liurui Xiao. (2025). Joint optimization of AI large and small models for surface temperature and emissivity retrieval using knowledge distillation. *Artificial Intelligence in Agriculture*, 15(3), 407-425. DOI:10.1016/j.aiaa.2025.03.009.



Joint optimization of AI large and small models for surface temperature and emissivity retrieval using knowledge distillation

Wang Dai^{a,b,1}, Kebiao Mao^{b,*,1}, Zhonghua Guo^a, Zhihao Qin^c, Jiancheng Shi^d, Sayed M. Bateni^e, Liurui Xiao^a

^a School of Electrical and Electronic-Engineering, Ningxia University, Yinchuan 750021, China

^b State Key Laboratory of Efficient Utilization of Arid and Semi-arid Arable Land in Northern China, Institute of Agricultural Resources and Regional Planning, Chinese Academy of Agricultural Sciences, Beijing 100081, China

^c School of Geographic Science and Planning, Nanning Normal University, Nanning 530001, China

^d National Space Science Center, Chinese Academy of Sciences, Beijing 100190, China

^e Department of Civil and Environmental Engineering and Water Resources Research Center, University of Hawaii at Manoa, Honolulu, HI 96822, USA

ARTICLE INFO

Article history:

Received 15 August 2024

Received in revised form 23 March 2025

Accepted 29 March 2025

Available online 12 April 2025

Keywords:

Artificial intelligence

Large models

Knowledge distillation

Automated machine learning

Remote sensing parameter retrieval

ABSTRACT

The rapid advancement of artificial intelligence in domains such as natural language processing has catalyzed AI research across various fields. This study introduces a novel strategy, the AutoKeras-Knowledge Distillation (AK-KD), which integrates knowledge distillation technology for joint optimization of large and small models in the retrieval of surface temperature and emissivity using thermal infrared remote sensing. The approach addresses the challenges of limited accuracy in surface temperature retrieval by employing a high-performance large model developed through AutoKeras as the teacher model, which subsequently enhances a less accurate small model through knowledge distillation. The resultant student model is interactively integrated with the large model to further improve specificity and generalization capabilities. Theoretical derivations and practical applications validate that the AK-KD strategy significantly enhances the accuracy of temperature and emissivity retrieval. For instance, a large model trained with simulated ASTER data achieved a Pearson Correlation Coefficient (PCC) of 0.999 and a Mean Absolute Error (MAE) of 0.348 K in surface temperature retrieval. In practical applications, this model demonstrated a PCC of 0.967 and an MAE of 0.685 K. Although the large model exhibits high average accuracy, its precision in complex terrains is comparatively lower. To ameliorate this, the large model, serving as a teacher, enhances the small model's local accuracy. Specifically, in surface temperature retrieval, the small model's PCC improved from an average of 0.978 to 0.979, and the MAE decreased from 1.065 K to 0.724 K. In emissivity retrieval, the PCC rose from an average of 0.827 to 0.898, and the MAE reduced from 0.0076 to 0.0054. This research not only provides robust technological support for further development of thermal infrared remote sensing in temperature and emissivity retrieval but also offers important references and key technological insights for the universal model construction of other geophysical parameter retrievals.

© 2025 The Authors. Publishing services by Elsevier B.V. on behalf of KeAi Communications Co., Ltd. This is an open access article under the CC BY-NC-ND license (<http://creativecommons.org/licenses/by-nc-nd/4.0/>).

1. Introduction

With the rapid development of artificial intelligence technologies, emerging methods such as Automated Machine Learning (AutoML) (He et al., 2021), large-scale models (Naveed et al., 2023), and knowledge distillation techniques (Gou et al., 2021) are propelling new trends across interdisciplinary research. These innovations not only meet the urgent needs of various industries for efficient and reliable solutions but also play a critical role in building universal models. Particularly in

the field of agricultural meteorological remote sensing parameter retrieval, the integration of traditional algorithms and artificial intelligence has opened new research perspectives and application prospects (Cao et al., 2023; Mei et al., 2023), showcasing superior performance compared to conventional methods (Yuan et al., 2020).

Current thermal infrared remote sensing technology still has room for further optimization in the retrieval of surface temperature and emissivity. By leveraging the latest AI technologies, new methods can be developed to enhance the accuracy of parameter retrieval. As technology advances and research deepens, this interdisciplinary integration is expected to drive the development of surface temperature and emissivity retrieval techniques, providing more precise data support for studies on agricultural meteorological disasters, crop growth, and yield assessments among other related fields (Moisa et al., 2022).

* Corresponding author.

E-mail addresses: maokebiao@caas.cn (K. Mao), qinzhizhao@caas.cn (Z. Qin), shijiancheng@nssc.ac.cn (J. Shi), smbateni@hawaii.edu (S.M. Bateni).

¹ These authors contributed equally to this work.

Traditional methods for surface temperature retrieval include the single-window, split-window, and multi-band algorithms that combine day and night observation data. Each of these methods has distinct features and has demonstrated significant value in practical applications (Wang et al., 2015). While these techniques generally provide reliable results in most scenarios, they still have limitations under specific environmental conditions. The single-window algorithm relies on the accuracy of prior knowledge of surface classification and atmospheric parameters during the retrieval process (Yu et al., 2014). The split-window algorithm estimates surface emissivity and atmospheric water vapor content based on surface type, effectively eliminating most atmospheric effects; however, its effectiveness depends on accurate parameter estimations (Frey et al., 2017). The multi-band algorithm, which assumes constant emissivity between day and night, requires adjustments in dynamically changing surface environments and is also influenced by observation angles (Wang et al., 2021a). Although these traditional algorithms perform well under various conditions, their limitations underscore the necessity and urgency of developing more precise and adaptable retrieval methods. To overcome these limitations of traditional remote sensing retrieval algorithms, an increasing number of studies are exploring the use of deep learning and other AI technologies for more accurate retrieval of remote sensing parameters such as surface temperature and emissivity (Mao et al., 2008; Yuan et al., 2020).

Deep learning (DL), as an advanced multilayer learning framework, has shown considerable potential in addressing complex nonlinear remote sensing inversion problems (Li et al., 2022; Mao et al., 2011). By learning intricate patterns and integrating various data types, deep learning not only deepens our understanding of the relationships among variables in remote sensing data but also significantly enhances the accuracy of surface temperature and emissivity retrievals through precise model training (Carter and Liang, 2019; Joshi et al., 2006; Mas and Flores, 2008). For instance, the use of Convolutional Neural Networks (CNNs) to retrieve Land Surface Temperature (LST) from Advanced Microwave Scanning Radiometer 2 (AMSR2) data has demonstrated deep learning's capability to handle the impacts of clouds and rainfall on synchronous ground observations (Tan et al., 2019). Studies on passive microwave satellite retrieval of LST also highlight the advantages of artificial intelligence in remote sensing technology, especially in complex surface environments like deserts (Duan et al., 2020; Li et al., 2023a). Deep learning algorithms exhibit robust capabilities in handling complex interactions of surface parameters. For example, a study using backpropagation neural networks to retrieve LST from Landsat 8 OLI/TIRS images has proven the superiority of neural networks in enhancing the precision of surface temperature retrievals (Zhang et al., 2021). Moreover, deep learning, by integrating physical models, statistical models, and expert knowledge, offers novel methods for multi-parameter inversion (Wang et al., 2021b). These methods not only extend the scope of artificial intelligence in handling complex parameter estimation problems but also optimize computational processes to enhance their physical interpretability, providing new paradigms for the remote sensing field (Wang et al., 2024). Further research has focused on reconstructing LST satellite datasets, predicting daily surface temperatures from time-series data, and fusing multi-source data to estimate sub-pixel surface temperatures (Jia et al., 2021; Wu et al., 2019; Yang et al., 2009). However, despite these significant technological breakthroughs based on traditional methods, these AI algorithms often fail to adequately consider the diversity of land cover, seasonal variations, and the specificities of different datasets, limiting their generalizability and application accuracy (Mao et al., 2023). Moreover, data-driven remote sensing inversion often relies on computationally intensive iterative processes to select neural network architectures in traditional exhaustive methods, limiting model scalability and complexity and resulting in high development cycles and computational resource consumption.

With the development of emerging artificial intelligence technologies like large models, knowledge distillation, and automated machine learning, traditional methods need to integrate these new technologies' advantages to enhance the accuracy and adaptability of remote sensing parameter inversion in complex data scenarios. This study leverages cutting-edge AI technologies to address the challenges posed by the complexity and nonlinear characteristics of the Earth system, solving the problem of limited accuracy in small model inversions due to the high complexity of data caused by diverse land covers. A new strategy called AutoKeras-Knowledge Distillation (AK-KD) integrates knowledge distillation technology for joint optimization of large and small models, establishing a methodological paradigm where large models facilitate the inversion of small models. Initially, the optimal neural network architecture for dataset inversion is obtained and trained using AutoKeras. Subsequently, a trained high-precision, generalizable large model serves as a teacher model, with a locally constrained small model as a student model. Pre-distillation using statistical indices verifies the best distillation weights, followed by formal knowledge distillation, where deep knowledge from the large model is transferred to the small model, enhancing its inversion accuracy in areas with limited precision and more closely approximating the actual physical characteristics. Finally, a high-accuracy parameter inversion model specific to certain areas is realized, and the student model is interactively integrated into the large model to form a high-quality joint optimization model, further enhancing the model's specificity and generalization capabilities.

2. Methodology

This study presents the AK-KD strategy, which combines physical and statistical methods as the theoretical foundation for remote sensing parameter inversion and integrates the following advanced artificial intelligence technologies to enhance both theoretical and practical application performance. Large models, utilizing massive training parameters and deep neural networks, exhibit significant potential in handling complex and high-dimensional data, crucial for improving the accuracy and adaptability of surface temperature and emissivity parameter inversion (Ananthaswamy, 2023). Knowledge distillation, an efficient model optimization strategy, focuses on extracting essential information and feature expressions from complex teacher models and transferring them to student models to optimize performance and achieve superior outcomes (Gou et al., 2021; Lin et al., 2021). The application of knowledge distillation in deep linear classifiers has been theoretically validated, revealing mechanisms by which student networks rapidly converge to generalization boundaries through distillation, elucidating the nature of student network learning and its convergence speed (Phuong and Lampert, 2019). Notably, knowledge distillation offers significant advantages over traditional model training methods (Wang and Yoon, 2021). By employing a knowledge distillation strategy, the teacher model demonstrates global generalization capabilities, effectively addressing the challenges faced by the student model in complex data scenarios, especially under topographically complex conditions. This approach enables small models to emulate the behavior of large models, excluding anomalous data in the inversion process, reducing background noise, improving feature extraction, and enhancing model generalizability, thereby elevating the performance of small models in specific application scenarios (Kelenyi et al., 2024), and at times surpassing that of large models (Furlanello et al., 2018). AutoKeras, an AutoML tool, generates models that can be conveniently exported as Keras models and deployed across various production environments within the TensorFlow ecosystem, achieving automation in model architecture selection and hyperparameter tuning, thereby effectively shortening the model development cycle and reducing computational resource consumption (Jin et al., 2023). By minimizing manual intervention and optimizing model structure, AutoKeras provides an

efficient and flexible solution suitable for data-driven remote sensing parameter inversion (Jin et al., 2019).

As shown in Fig. 1, the key technologies of this strategy comprise five parts: The first part involves physical logic reasoning (Fig. 1A), which uses physical inversion algorithms to derive the logical relationships between output and input parameters, thus identifying the band parameters for input nodes. This, built on generalized statistical methods based on physical approaches, provides theoretical support for large model training to handle high-dimensional, diverse sample data; the second part employs the automatic machine learning tool AutoKeras to optimize the model structure (Fig. 1B), effectively selecting the most

suitable neural network architecture for specific datasets using the data-driven characteristics of remote sensing parameter inversion; the third part is knowledge distillation (Fig. 1C), where the optimal neural network architecture is selected on preprocessed data for model training, and a high-accuracy large model serves as a teacher model to enhance a smaller model, thereby boosting its performance; the fourth part details the knowledge transfer process (Fig. 1D), explaining how the knowledge from the teacher model is transferred to the student model, optimized through a weighted fusion; the fifth part is validation (Fig. 1E), which involves a comprehensive verification of the AK-KD strategy's effectiveness, including theoretical validation, cross-

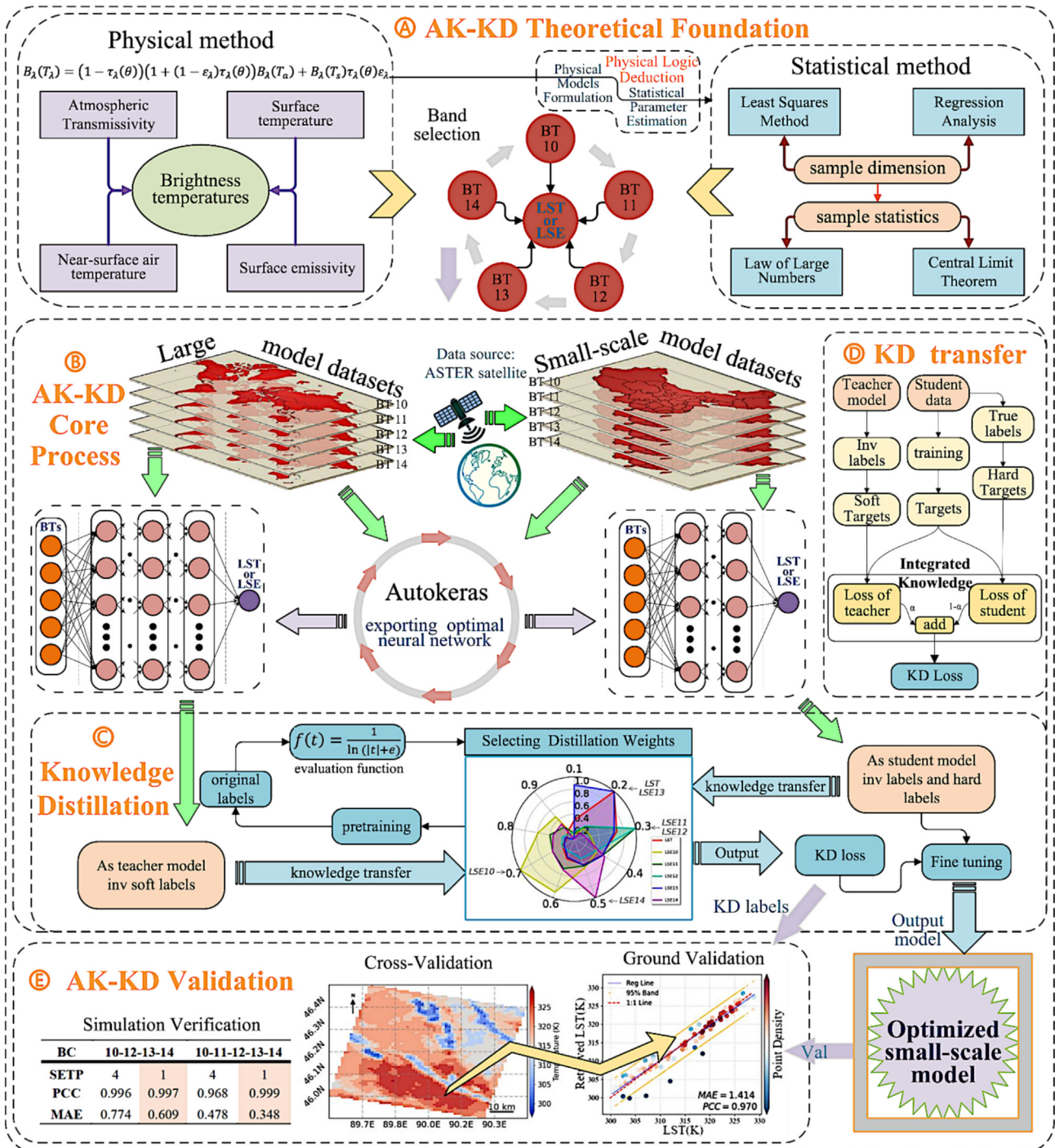


Fig. 1. Detailed flowchart of the AK-KD strategy.

validation, and ground validation to ensure the reliability and efficacy of the proposed strategy. Further details of each part will be elaborately discussed below.

2.1. Theoretical derivation of parameter inversion

In addressing problems using deep learning, it is essential first to undertake physical logic reasoning to provide a sound basis for utilizing deep learning optimally. Physical logic derivations construct physical methodologies, upon which generalized statistical methods are developed. These physical and statistical methods representatively deconstruct into the foundational training and testing data for deep learning, thereby facilitating the coupling of deep learning with physical and statistical methodologies (as shown in Fig. 1A). For detailed theoretical derivations on how deep learning couples with physical and statistical methods, refer to references (Mao et al., 2007; Mao et al., 2024).

Initially, physical methods provide the necessary theoretical foundation for practical applications. The interdependencies among geophysical parameters determine that inversion algorithms must satisfy three conditions: first, the inversion model must be physically meaningful; second, the inversion equations should be mathematically solvable in theory; third, the inversion must be highly accurate to meet the demands of practical applications. In the process of surface temperature inversion, this is based on the surface thermal radiation and the transmission of ground thermal radiation through the atmosphere to the remote sensing satellite (Mao et al., 2024). The Radiative Transfer Equation (RTE) plays an indispensable role in this process, providing a theoretical framework for the propagation of surface thermal radiation through the atmosphere, crucial for accurate analysis and simulation of this complex physical process. The RTE is expressed as follows:

$$B_{\lambda}(T_{\lambda}) = (1 - \tau_{\lambda}(\theta))(1 + (1 - \varepsilon_{\lambda})\tau_{\lambda}(\theta))B_{\lambda}(T_a) + B_{\lambda}(T_s)\tau_{\lambda}(\theta)\varepsilon_{\lambda} \quad (1)$$

The Planck function is defined as:

$$B_{\lambda}(T) = \frac{2hc^2}{\lambda^5} \frac{1}{e^{(hc/\lambda kT)} - 1} \quad (2)$$

In the RTE, $B_{\lambda}(T_{\lambda})$ represents satellite radiation, $\tau_{\lambda}(\theta)$ atmospheric transmissivity, T_s surface temperature, T_a near-surface air temperature, and ε_{λ} surface emissivity. In the Planck function, λ represents wavelength, e is the Euler's number, 2.71828, c is the speed of light, 3×10^8 (m·s⁻¹), h is Planck's constant, 6.63×10^{-34} (J·s), and k is the Boltzmann constant, 1.38×10^{-23} (J·K⁻¹). In this set, $\tau_{\lambda}(\theta)$, T_s , T_a , ε_{λ} are unknowns, thus theoretically requiring at least four TIR bands to establish four RTE equations to invert LST and LSE. Physical equation sets need simplification due to each term containing a Planck function, thereby introducing errors. To significantly enhance parameter inversion accuracy, employing deep learning for optimization calculations can effectively eliminate atmospheric interference from remote sensing data.

Next, generalized statistical methods based on physical methodologies are constructed to gather more samples from multi-source data, enhancing the model's practicality and inversion accuracy. Bubeck and Sellke mathematically demonstrated that increasing the number of parameters in a model enhances robustness and thus generalizability (Bubeck and Sellke, 2023). In the realm of data fitting, introducing more data volume and expanding equation dimensions are key strategies to enhance model fitting accuracy. In terms of data dimensions, incorporating more feature variables enriches the model's foundational information. Specifically, by applying least squares to minimize the total error squared $S = \sum_{i=1}^n (y_i - \hat{y}_i)^2$ (where y_i is the predicted value, \hat{y}_i is the model's predicted value), model parameters are optimized, enhancing fitting accuracy. Regression analysis further expands

this framework by solving $\hat{\beta} = (X^T X)^{-1} X^T y$ (where X is the design matrix, y the response vector), thus expanding observation sample dimensions and allowing precise model parameter adjustments within the framework of minimizing error squared. Regarding sample size, based on the Law of Large Numbers, as the sample size n approaches infinity, the sample mean $\bar{X}_n = 1/n(\sum_{i=1}^n X_i)$ converges in probability to the population mean μ , $P(|\bar{X}_n - \mu| > \epsilon) \rightarrow 0$. The increase in sample size causes the model's sample mean to gradually approach the population mean, further enhancing the model's generalizability. According to the Central Limit Theorem, as the sample size increases, the distribution of the sample mean approaches a normal distribution, $\sqrt{n}(\bar{X}_n - \mu) \sim \mathcal{N}(0, \sigma^2)$. This approximation to a normal distribution provides a foundation for using statistical methods (such as hypothesis testing and confidence intervals) to enhance model reliability in assessing and predicting unknown data, significantly improving the model's generalizability. Through this integration of physical and statistical methods, maintaining an appropriate balance between model complexity and data volume provides a solid theoretical foundation for model training in the AK-KD algorithm.

2.2. Automated machine learning strategy

Under the framework of joint model optimization, the selection of automated parameter search techniques directly influences the balance between model performance and computational efficiency. Current optimization strategies in academia can be categorized into two types: heuristic parameter tuning based on swarm intelligence (such as the Spider Monkey Optimization algorithm, SMO), and architecture search based on probabilistic surrogates (such as Bayesian Optimization-driven Neural Architecture Search). For instance, the Bi-LSTM fusion model employs the SMO algorithm, which simulates swarm collaboration mechanisms to globally optimize low-dimensional continuous spaces, significantly enhancing the robustness of bus passenger flow prediction (Balasubramani and Natarajan, 2024). However, in complex scenarios requiring exploration of high-dimensional discrete spaces (such as combinations of neural network layers and connection methods), Bayesian-driven NAS is more suitable for handling joint discrete optimization of structures and hyperparameters. Addressing this issue, this study selects the AutoKeras framework, which utilizes Bayesian Optimization's probabilistic surrogate model to guide Neural Architecture Search (NAS) directionally. By dynamically evaluating the posterior distribution of candidate network structures, it rapidly identifies the optimal model architecture. As an implementation of AutoML, AutoKeras focuses on automatically identifying the most suitable model structures and hyperparameters through Neural Architecture Search (NAS), thereby optimizing the performance of deep learning models. Its core advantage lies in the dual constraint mechanism coupling Bayesian Optimization with Gaussian Processes. Specifically, Bayesian Optimization drives Neural Architecture Search to identify key structural features, while Gaussian Processes control the degree of network deformation through probabilistic modeling, ensuring efficient convergence within the predefined search space (Jin et al., 2019).

The problem of neural structure search can be described as follows: Given a neural structure search space \mathcal{S} , divide input data D into training data D_t and validation data D_v , and evaluate the efficiency of neural network architectures using a cost function. The objective is to find an optimal neural network $f \in \mathcal{S}$ that achieves the best performance on dataset D . Therefore, the search seeks to find the optimal neural network f and its learning parameters θ that satisfy:

$$f = \min_{f \in \mathcal{S}} \text{Cost}(f(\theta), D_v) \quad (3)$$

$$\theta = \min_{\theta} \mathcal{L}(f(\theta), D_t) \quad (4)$$

here, Cost is an evaluation metric (such as correlation coefficient or absolute error), and θ represents the learning parameters of f . The search space SSS covers all neural network architectures by progressively adjusting the initial architecture and is specifically described as:

$$\mathcal{S} = \{n, \{(u_i, \phi_i, p_i)\}_{i=1}^n\} \quad (5)$$

where n is the number of layers in the neural network, u_i is the number of units in layer i , ϕ_i is the activation function for layer i , and p_i is the dropout probability for layer i , ranging from $[0,1]$. Under the guidance of Bayesian optimization, the system searches within space \mathcal{S} for the best architecture.

In the AK-KD strategy, data collected from the ASTER satellite are first preprocessed, then fed into the AutoKeras system. AutoKeras employs a Bayesian optimization-based neural architecture search (NAS) to determine the optimal neural network structure suited to the data, which is then used for formal training, as detailed in part B of Fig. 1. Within AutoKeras, a basic search space, FCN, is defined with parameters including: the number of neural layers $n \in N \cap [3, 9]$, the number of neurons per layer $u_i \in N \cap [32, 1024]$ with a search step of 16, activation functions $\phi_i \in \{\text{ReLU}, \text{Tanh}, \text{Sigmoid}\}$, and dropout ratio $p_i \in [0, 0.5]$ with a search step of 0.1. The schematic diagram of its neural network is shown in Fig. 2:

After data input, the initial stage involves pre-training the model with a lower number of epochs to validate the effectiveness of each searched neural network architecture. During the search process, network deformation is controlled through Gaussian processes and Bayesian optimizers, allowing the system to efficiently explore the predefined search space. The neural network kernel function based on edit distance is defined as:

$$\kappa(f_a, f_b) = e^{-\rho^2(d(f_a, f_b))} \quad (6)$$

where $d(f_a, f_b)$ represents the edit distance between two neural networks, and ρ is a mapping function. The kernel function, by evaluating the similarity between different neural network architectures, guides the network transformation during the search. After a set number of searches, the system automatically terminates the search and outputs the optimal neural network architecture. Finally, the optimal architecture is used for formal training to achieve the best performance model.

2.3. Theoretical derivation of knowledge distillation networks

In the realm of deep learning, a model's scale, complexity, and performance typically serve as pivotal metrics for evaluating its practical utility. Knowledge distillation addresses the intricate balance between

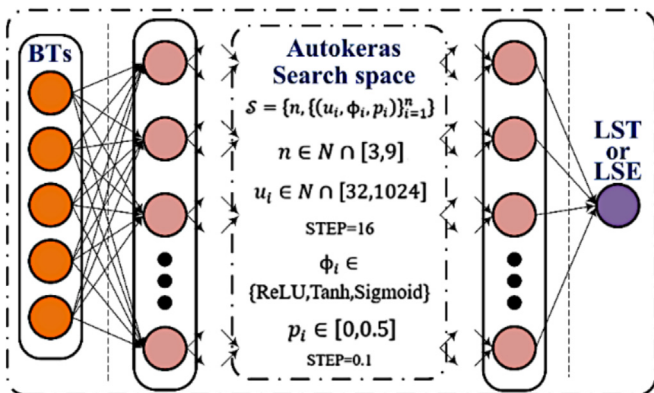


Fig. 2. Schematic of the neural network training model for AutoKeras.

model complexity and performance by constructing a “teacher–student” transfer framework (Wang and Yoon, 2021). This technique not only extracts deep knowledge from complex models but also transcends traditional training’s reliance on annotated data, enabling lightweight models to inherit the decision-making logic of their teacher counterparts. However, in cross-domain scenarios, conventional methods constrained by the homogeneous domain assumption (identical distributions for source and target domains) often result in failed static feature alignment, severely limiting knowledge transfer efficiency. To address this, Tang et al. (2023) proposed a dynamic distribution alignment paradigm: the KD³ algorithm innovates a hybrid distribution contrastive learning mechanism, integrating perturbed sample generation and dynamic instance weighting strategies to establish a more robust knowledge calibration system. The subsequently developed the 4Ds framework employs Fourier frequency domain decoupling to disentangle domain-invariant phase components (global semantics) from domain-specific amplitude features (local styles), achieving dynamic domain adaptation through residual adapters (Tang et al., 2024). Knowledge distillation technology effectively balances model performance and complexity in cross-domain scenarios by dynamically optimizing domain adaptation strategies and contrastive learning mechanisms, thereby reducing reliance on homogeneous data distributions. Furthermore, research highlights critical factors influencing distillation success: dynamic data distribution alignment, bias–variance trade-off optimization in distillation objectives, and the alignment of feature extraction capabilities between student and teacher model.

In practical applications, response-based distillation strategies are employed, focusing primarily on the neural responses of the teacher model’s last layer, aiming to directly learn the teacher model’s final predictions (Gou et al., 2021). Specifically, large models with strong generalization capabilities and high accuracy serve as teacher models, guiding smaller models to learn and mimic the prediction behavior of large models, ultimately resulting in efficient student models. Through this method, small models use the large model’s predictions as soft labels to generate similar predictions for the same inputs, thereby emulating the large model’s behavior (Hinton et al., 2015). The distillation loss for response-based knowledge transfer is expressed as:

$$L_{\text{Res}}(p(z_t, T), p(z_s, T)) = \mathcal{L}_{\mathcal{R}}(p(z_t, T), p(z_s, T)) \quad (7)$$

where $\mathcal{L}_{\mathcal{R}}$ represents the evaluation loss. z_s is the output of the small model, z_t is the output of the large model, and T is a factor controlling the importance of z_t . In this research framework, Mean Squared Error (MSE) is used as the specific implementation of the loss function L , chosen for its favorable performance in convex optimization and nonlinear regression models. MSE is defined as the average squared difference between observed values y and predicted values \hat{y} , where N is the number of samples. This metric provides an effective way to quantify model prediction accuracy. The precise expression of MSE is as follows:

$$\text{MSE}(y, \hat{y}) = \frac{1}{N} \sum_{i=1}^N (y_i - \hat{y}_i)^2 \quad (8)$$

To construct a comprehensive and integrated optimization objective, a Global Optimization Criterion (GOC) is introduced on top of the distillation loss to calculate knowledge distillation training, as shown in the following equation. This criterion is a weighted sum that merges two key metrics: Data Fidelity (\mathcal{L}_D) and Model Consistency (\mathcal{L}_M):

$$\text{GOC}(y, \hat{y}_t, \hat{y}_s, \alpha) = \alpha \mathcal{L}_D(y, \hat{y}_s) + (1 - \alpha) \mathcal{L}_M(\hat{y}_t, \hat{y}_s) \quad (9)$$

here, the weight parameter α is a tunable parameter between 0 and 1, used to balance the relative contributions of these two metrics in the overall optimization objective. Data Fidelity focuses on minimizing the difference between true outputs y and the student model’s predictions \hat{y} . Model Consistency primarily aims to minimize the output differences between the large model (\hat{y}_t) and the small model (\hat{y}_s).

$\mathcal{L}_D = \text{MSE}(y, \hat{y})$ quantifies the difference between the small model's output and the true labels, while $\mathcal{L}_M = \text{MSE}(\hat{y}_t, \hat{y}_s)$ quantifies the difference between the outputs of the small and large models. Thus, the small model in training seeks to closely emulate the large model while also closely aligning with the true labels.

Knowledge distillation is also widely applied to achieve label smoothing, evaluate teacher model accuracy, and determine the optimal output layer structure (Gou et al., 2021), including enhancing the entropy of labels during the data demonstration process to effectively boost the model's prediction capabilities (Bagherinezhad et al., 2018). Therefore, under the framework of knowledge distillation, further exploration has been conducted on applying knowledge transfer to the concept of training data compression, termed dataset distillation. By integrating the critical knowledge of large datasets into smaller, more efficient student datasets with certain distillation weights, the aim is to alleviate the burden of deep model training. In the knowledge distillation process for small models, particularly in the application to surface temperature datasets, adjustments via knowledge distillation weight factors are made to correct dataset distillation under ideal clear-sky conditions, bridging the gap between actual and predicted values (Li et al., 2023b). This provides accurate empirical values for surface temperature inversion under data complexity-limited conditions, ultimately forming an efficient student model.

Specifically, during the knowledge distillation process, the most suitable knowledge distillation weights within the global optimization strategy are first identified, as illustrated in Fig. 1C. The preliminary phase adopts a pre-distillation approach, using the large model to provide preliminary guidance to the small model. During this process, direct distillation of datasets is omitted, using PCC and MAE as key evaluation indices to explore a weight range of 0.1 to 0.9, conducting a series of pre-distillation experiments for small models' surface temperature and emissivity (LST, LSE10–14) based on statistical tests to determine the optimal knowledge distillation weights. Subsequently, the selected weights are applied in the formal distillation process, where the large model optimizes the small model incrementally during each iteration based on the knowledge distillation loss generated by the global optimization strategy. Following this, dataset distillation for the small model is performed using the determined knowledge distillation weights to achieve high-quality dataset optimization reconstruction. This method merges the soft targets of the large model with the hard targets of the small model into composite labels. These labels not only retain the original category information but also incorporate the large model's understanding of the data's underlying structure, providing the small model with a richer training target. Using these composite labels, the training of the small model is no longer limited to pursuing consistency with hard targets but approaches a more detailed and comprehensive objective, including recognizing and simulating the subtle interrelations between categories revealed by the large model. This comprehensive mechanism injects a more refined and comprehensive supervisory signal into the training of the student model, promoting improvements in model accuracy and generalization capability.

This strategy not only enables the small model to inherit the decision-making capabilities of the large model but also significantly enhances performance while maintaining low complexity and computational costs, even surpassing the large model. This process effectively bridges the gap between model predictions and actual values, ensuring high accuracy in inversion results, demonstrating the significant advantages of knowledge distillation technology in enhancing data inversion accuracy, ultimately forming an efficient student model, further ensuring that the small model's surface temperature and emissivity inversion results closely align with the physical characteristics' representations.

2.3.1. Selection of knowledge distillation weights

In the process of knowledge distillation, weight optimization is one of the core issues, determining the intensity of knowledge

transfer between the teacher and student models, and directly affecting the student model's ability to assimilate the teacher model's knowledge while retaining its own learning characteristics, as illustrated in Fig. 1D. Theoretically, seeking an ideal alpha value aims to achieve the best balance between teacher guidance and student autonomous learning without sacrificing the student model's adaptability while maximizing the guidance benefits obtained from the teacher model. This process emphasizes the dynamic balance between the student model's self-exploration capabilities at lower alpha values and the guiding role of the teacher model at higher alpha values, with the key being to find an optimal alpha value to facilitate the effective integration of teacher guidance and student autonomous exploration, thereby enhancing the student model's performance on specific tasks.

Theoretically, after initial training completion, utilizing original data for incremental learning of the model can continuously garner useful knowledge, achieving further precision enhancements (Luo et al., 2020). The selection of knowledge distillation weights leverages this characteristic by considering only the original labels for student model distillation, not extra knowledge distillation labels. Under such circumstances, when the knowledge distillation weight is zero, meaning no guidance from the teacher model is introduced, it equates to incremental learning, and the student model's accuracy improves. However, when the weight is one, implying total reliance on the teacher model, it deviates from the incremental learning of the original dataset, causing accuracy to decline due to training loss deviations from the original labels (Mittal et al., 2021). Hence, seeking a dynamic balance point where both the teacher model's contribution and the student model's contribution act together is crucial, followed by using this weight to officially optimize the student model under the knowledge distillation labels.

Within this framework, the independent sample *t*-test is utilized to compare the mean differences between two independent sample groups (i.e., original accuracy and adjusted weight accuracy). The goal is to find the weight with the lowest *t*-value, i.e., the dynamic balance point of knowledge distillation contribution. The formula for calculating the *t*-statistic is as follows:

$$t = \frac{\bar{x}_1 - \mu}{\frac{s_1}{\sqrt{n_1}}} \tag{10}$$

where \bar{x}_1 represents the sample mean of improved accuracy, μ is the accuracy before improvement, s_1^2 is the sample standard deviation of improved accuracy, and n_1 is the sample size. To further analyze the contributions of different weights to the final model accuracy enhancement, the relative utility of weights is quantified through the statistical *t*, and the evaluation function is designed as:

$$f(t) = \frac{1}{\ln(|t| + e)} \tag{11}$$

To deepen the understanding of the distribution of the *t*-statistic under given degrees of freedom, the probability density function (PDF) of the *t*-distribution is introduced as follows:

$$f(t) = \frac{\Gamma(\frac{v+1}{2})}{\sqrt{v\pi}\Gamma(\frac{v}{2})} \left(1 + \frac{t^2}{v}\right)^{-\frac{v+1}{2}} \tag{12}$$

here, v represents degrees of freedom, and Γ is the gamma function, used to extend the concept of factorial in this context. Further, the cumulative distribution function (CDF) of the *t*-distribution provides the probability of observing a specific *t*-value or more extreme values:

$$F(t) = \int_{-\infty}^t f(u) du \tag{13}$$

Combining the t-statistic and its degrees of freedom, and determining p -values through the CDF of the t-distribution, which represents the probability of observing the calculated statistic (or a more extreme case) under the assumption that the null hypothesis is true. For a two-tailed test, the formula for calculating the p -value is:

$$p = 2 \times (1 - F(|t|)) \quad (14)$$

In summary, this section, through an in-depth analysis of the knowledge distillation weight selection mechanism, establishes a theoretical basis for effective knowledge transfer between large and small models. By precisely adjusting weight parameters, this study aims to balance the relationship between large model guidance and small model self-learning, thereby achieving an optimal learning pathway for the student model.

3. Data and study area

3.1. Large model dataset

In this study, data from the Advanced Spaceborne Thermal Emission and Reflection Radiometer (ASTER) were utilized, characterized by its high spatial resolution and multispectral capabilities, allowing for a more detailed depiction of surface features. We selected high-quality summer ASTER data covering the primary land surface types in China to ensure the dataset's comprehensiveness and representativeness. A diversified strategy was adopted, collecting approximately 9.6 million samples across 27 scenes, which provided a solid foundation for building a large model with high generalization ability and ensured balanced performance across various types of data. To guarantee data quality, all samples underwent stringent quality control and preprocessing. Combining MODIS data, ground observation data, and assimilation data, ASTER data consistent with high-reliability data were carefully selected to ensure accuracy. We ensured the model's generalization capability and accuracy by pre-training evaluations of each preprocessed scene, selecting datasets with high inversion precision for inclusion in the large model training repository.

3.2. Small model data

During the selection phase for the large model data in this study, two scenes were specifically chosen due to their complex terrain, which caused low inversion accuracy. Complex terrain is a relative concept. In our context, it typically refers to areas with intricate topography and significant variations in surface types, such as mountainous regions or urban environments. From the visible imagery, it is evident that these areas feature diverse surface types and significant topographical variations, making them key cases for optimizing the small model. These areas' data are limited by the inherent complexity and nonlinear characteristics of the Earth system, directly affecting the small model's inversion accuracy. These specific scenarios provide a suitable environment for utilizing knowledge distillation technology to analyze and enhance the performance of the small model. Through this process, the study aims to explore the adaptability and optimization methods of the small model under conditions of data complexity and limited accuracy, laying the groundwork for subsequent model evaluation and application research.

3.3. Auxiliary data

3.3.1. MODIS data

In this study, MODIS surface temperature data were used as a key auxiliary dataset for cross-validation to ensure the reliability and precision of the model inversion results. Specifically, MODIS surface temperature data corresponding to the spatial and temporal points of the two small models were carefully selected as the benchmark for cross-

validation. This selection aimed to evaluate and optimize model performance, ensuring its accuracy and robustness across different temporal and spatial scales.

3.3.2. Ground data

This study utilized ground data to validate the accuracy of models trained on the ASTER dataset. Within the two target study areas, areas with flat terrain and homogeneous surface types were selected to collect a series of high-quality ground observation data. Given the broader availability of surface temperature data compared to emissivity, this study focused on comparing the surface temperature data inverted by the optimized student model with ground measurement values to verify the effectiveness of the proposed methods. The alignment of ground data with ASTER satellite observations in space and time ensured the rigor and accuracy of the validation process.

4. Results and discussion

The computational resources utilized in our experiments are as follows: The operating system employed was Ubuntu 22.04 LTS, with a deep learning framework version of 2.17.0. The Python programming language version used was 3.10.13. For central processing, we utilized an Intel(R) Xeon(R) Platinum 8474C CPU, complemented by 80GB of RAM. Graphics processing was handled by an RTX 4090D GPU, equipped with 24GB of dedicated memory.

4.1. Theoretical accuracy analysis and validation

4.1.1. Automated machine learning network optimization

During the process of remote sensing inversion using deep learning, the selection of neural network architectures often relies on exhaustive trial-and-error methods, and the configuration of neurons between layers lacks flexibility. In response, this study adopted the AutoKeras automated network search framework, conducting 30 iterative searches within a predefined search space to explore optimal network architectures. The Pearson Correlation Coefficient (PCC) and Mean Absolute Error (MAE) were used as performance metrics for the models. MAE was chosen because it intuitively reflects the average deviation between predicted values and true values, serving as a commonly used tool to measure prediction accuracy. PCC was used to assess the linear correlation between predicted values and actual values, aiding in revealing the correlation strength between model outputs and real data, thus providing a deeper assessment of the model's explanatory power. By integrating these two metrics, the model's absolute error could be evaluated, and the correlation level between model predictions and actual outcomes assessed, allowing for a comprehensive evaluation of model performance. Specifically, the search for the optimal neural network architecture was conducted using large model surface temperature inversion data, demonstrating AutoKeras's search efficiency and configuration flexibility through eight neural network architecture searches across 30 epochs. The results include the number of layer neurons, activation function (act. func.) and other model configuration information, with specific results shown in [Table 1](#).

Analysis of the results indicated that the third attempt, which included a neural network architecture with seven hidden layers (32, 32, 720, 32, 32, 752, 32), achieved higher accuracy in large model LST inversion, and thus this architecture was chosen for large model LST inversion tasks. Given the data-driven nature of the inversion model, AutoKeras will be used in subsequent inversion tasks to derive the best neural network architecture for more targeted training, aiming to achieve optimal accuracy.

4.1.2. Input band selection and validation

Through the physical logic analysis discussed in [Section 2.1](#), to construct a closed system of equations, the number of equations must be at least equal to the number of unknowns; thus, for ASTER data, at

Table 1
Optimal neural network architecture search for large model LST inversion using AutoKeras.

	Trial 1	Trial 2	Trial 3	Trial 4	Trial 5	Trial 6	Trial 7	Trial 8
Layer 1	32	32	32	880	784	272	769	288
act. func.	Relu	Tanh	Tanh	Relu	Relu	Relu	Relu	Relu
Layer 2	1024	32	32	864	976	464	576	464
act. func.	Relu							
Layer 3	32	32	720	32	32	192	32	224
act. func.	Relu	Relu	Relu	Relu	Relu	Tanh	Relu	Sigmoid
Layer 4	32	32	32	32	400	32	704	32
act. func.	Relu							
Layer 5	32	32	32	32	32	32	336	32
act. func.	Sigmoid	sigmoid	Relu	Relu	Relu	Relu	Relu	Relu
Layer 6	880	32	752	32		32	32	
act. func.	Relu	Relu	Relu	Relu		Relu	Relu	
Layer 7	32	32	32				448	
act. func.	Relu	Relu	Relu				Tanh	
Layer 8	32						848	
act. func.	Sigmoid						Relu	
dropout	0.25				0.25			
optimizer	Adam	Adamw	Adam	Adam	Adam	Adam	Adam	Adamw
PCC	0.968	0.968	0.978	0.969	0.968	0.969	0.968	0.969
MAE	0.679	0.668	0.668	0.976	0.693	0.687	0.676	0.661

least four thermal infrared bands are necessary to construct the system. This implies that in a deep learning neural network, the number of input nodes should at least correspond to four thermal infrared bands. To validate this theory, this study considered all possible band combinations from single to multiple bands, initially using ASTER simulated datasets with a surface temperature step of 4, selecting all possible combinations of the five brightness temperature bands BT10 ~ 14 for input. Models were trained and surface temperature inversion experiments

conducted using AutoKeras neural network searches. MAE and PCC were used as evaluation metrics to explore the relationship between input band combinations and model accuracy. A comprehensive analysis of band combinations (BC) not only helps reduce overall model errors and enhances prediction accuracy but is also a key step in establishing an effective model. Detailed experimental results are seen in Table 2, clearly illustrating the specific impacts of different combinations on model accuracy.

Table 2
Relationship between input band combinations and model accuracy.

IBC	10	11	12	13	14
PCC	0.952	0.952	0.951	0.965	0.966
MAE	3.520	3.420	3.386	2.995	2.943
3BC	10-11	10-12	10-13	10-14	11-12
PCC	0.965	0.968	0.978	0.974	0.961
MAE	2.204	2.686	2.232	2.489	2.878
3BC	11-13	11-14	12-13	12-14	13-14
PCC	0.981	0.981	0.985	0.984	0.980
MAE	2.201	2.132	1.901	1.963	2.032
3BC	10-11-12	10-11-13	10-11-14	10-12-13	10-12-14
PCC	0.969	0.959	0.982	0.964	0.991
MAE	1.451	1.113	1.236	1.244	1.349
3BC	10-13-14	11-12-13	11-12-14	11-13-14	12-13-14
PCC	0.931	0.991	0.990	0.990	0.991
MAE	1.598	1.307	1.395	1.410	1.342
4BC	10-11-12-13	10-11-12-14	10-11-13-14	10-12-13-14	11-12-13-14
PCC	0.865	0.979	0.968	0.996	0.96
MAE	0.663	0.827	0.708	0.774	0.875
5BC			10-11-12-13-14		
PCC			0.968		
MAE			0.478		

In-depth analysis of surface temperature inversion validated the theoretical expectations that increasing band combinations significantly enhances model performance. Firstly, PCC analysis indicated that performance improvement is not solely dependent on an increase in the number of bands. For example, in 1 BCE, band 14 exhibited the best PCC at 0.966, in 2 BCE, bands 11–13 (PCC 0.981), and in 3 BCE, bands 12–13–14 (PCC 0.991) showed higher PCCs, even surpassing some four and five-band combinations, although their MAEs were less satisfactory. This highlights the critical role of information complementarity of selected bands on model accuracy. Secondly, MAE analysis showed that multi-band combinations further optimized performance, particularly the 10–12–13–14 combination with a PCC of 0.996 and MAE of 0.774. The exemplary performance of the five-band combination 10–11–12–13–14 with a PCC of 0.968 and MAE of 0.478 emphasized the importance of integrating multi-band information for precision improvement, thus substantially supporting the initial theoretical analysis. Considering both PCC and MAE, preliminary selections were made for 4 10–12 BCE–13–14 and 5 10–11 BCE–12–13–14 band combinations.

To validate the Law of Large Numbers and explore the impact of sample size on model performance, sample data was increased and surface temperature steps reduced to 1, selecting the more effective band combinations (4 10–12 BCE–13–14, 5 10–11 BCE–12–13–14) from Table 2 as experimental subjects. To further assess the impact of sample volume on inversion accuracy, these results were compared with the inversion accuracy of simulation data at a step of 4, with detailed results shown in Table 3:

The analysis showed that by reducing the step to expand sample volume, the accuracy of the surface temperature inversion model significantly improved. When the step decreased from 4 to 1 and sample data increased fourfold, the inversion accuracy PCC for the four-band combination 10–12–13–14 improved from 0.996 to 0.997, and MAE decreased from 0.774 K to 0.609 K. The five-band combination 10–11–12–13–14 saw its PCC increase from 0.968 to 0.999, and MAE decrease from 0.478 K to 0.348 K, serving as a simulated validation for large model training under the AK-KD strategy. This trend confirmed that increasing sample volume under certain data quality conditions contributes to enhancing model accuracy.

4.2. Dataset model training and analysis

Based on the data and study area introduction, the large model refers to a high-accuracy model trained using the large model dataset. The small model refers to models trained on small model data with accuracy lower than the large model, and the student model refers to small models optimized using knowledge distillation.

4.2.1. Large model training and analysis

In this study, neural network architectures determined by AutoKeras were used to train selected large model datasets, aiming to precisely invert Land Surface Temperature (LST) and emissivity for brightness temperature bands (BT10, BT11, BT12, BT13, BT14). This process led to the construction of independent inversion models for each target, producing scatter plots and accuracy displays (as shown in Fig. 3) to visually demonstrate model performance, where the color bands on the right indicate relative point density.

Specifically, the obtained inversion models performed as follows: the LST model had a Pearson Correlation Coefficient (PCC) of 0.967

and a Mean Absolute Error (MAE) of 0.691 K, indicating good correlation and reasonable error levels; the emissivity models for bands LSE10 to LSE14 had PCCs of 0.932, 0.948, 0.950, 0.844, and 0.782 respectively, with similarly low MAEs ranging from 0.007 to 0.001. These results support the use of the large model as a teacher model, with its multi-input features and large data volume contributing to model accuracy, also validating the effectiveness of the chosen neural network architecture and revealing performance differences between the band inversion models. This progress lays a solid foundation for using knowledge distillation technology to enhance the accuracy of small models.

4.2.2. Small model training and analysis

In this study, neural network architectures selected by AutoKeras were used for surface temperature and emissivity inversion analysis on two small model cases. Scatter plots and accuracy displays for small models 1 and 2 are shown in Figs. 4 and 5, respectively. These small model datasets originated from datasets with limited inversion accuracy due to complex data, constrained by the inherent complexity and nonlinear characteristics of the Earth system. Compared to the high-quality large dataset models, small models 1 and 2 showed performance gaps in key performance indicators PCC and MAE, especially evident in specific bands such as LSE13 and LSE14. This comparison highlights the impact of data quality and volume on inversion accuracy and also emphasizes the potential of knowledge distillation technology in enhancing the performance of small models, providing new insights for model applications in complex environments.

4.2.3. Large model analysis on small model data

This section delves into the analysis of large model inversion on small model data. Large model data, based on a composite of multiple partitioned data, reflects the overall accuracy of global partition data, approximating the average inversion accuracy of partition models. However, for small models trained on certain precision-limited partition data, their inversion accuracy falls below the global average, i.e., below the large model's accuracy. Although the large model can integrate global data, capture more complex nonlinear features, and minimize global errors, the accuracy limitations of specific partition data may prevent ideal accuracy in these partitions' inversion results. To verify this, the LST & LSE of two precision-limited small models were inverted using the large model, with scatter plots and displays shown in Figs. 6 and 7.

The large model achieved a PCC of 0.967 and MAE of 0.691 K in LST inversion. In contrast, small model 1 had a PCC of 0.970 and MAE of 1.099; small model 2 had a PCC of 0.948 and MAE of 1.029. When using the large model to invert small model data, the results for small model 1 showed an MAE of 1.529 and PCC of 0.966; for small model 2, an MAE of 1.091 and PCC of 0.943. These results indicate that, although the large model has higher global inversion accuracy, its performance on precision-limited small model data generally has lower PCC than the small models' own inversion results. For MAE, the accuracy is also below that of the small models' own results, particularly the large model's inversion of small model 1 data showed a significantly higher MAE. Results for LSE10 ~ 14R also displayed similar trends, where the large model's global accuracy exceeded the small models' own data inversion accuracy, which in turn was higher than the large model's accuracy on small model data. These findings confirm that despite the large model's high global accuracy, its inversion accuracy remains suboptimal

Table 3
Relationship between sample data and model accuracy.

BC	10-12-13-14		10-11-12-13-14	
SETP	4	1	4	1
PCC	0.996	0.997	0.968	0.999
MAE	0.774	0.609	0.478	0.348

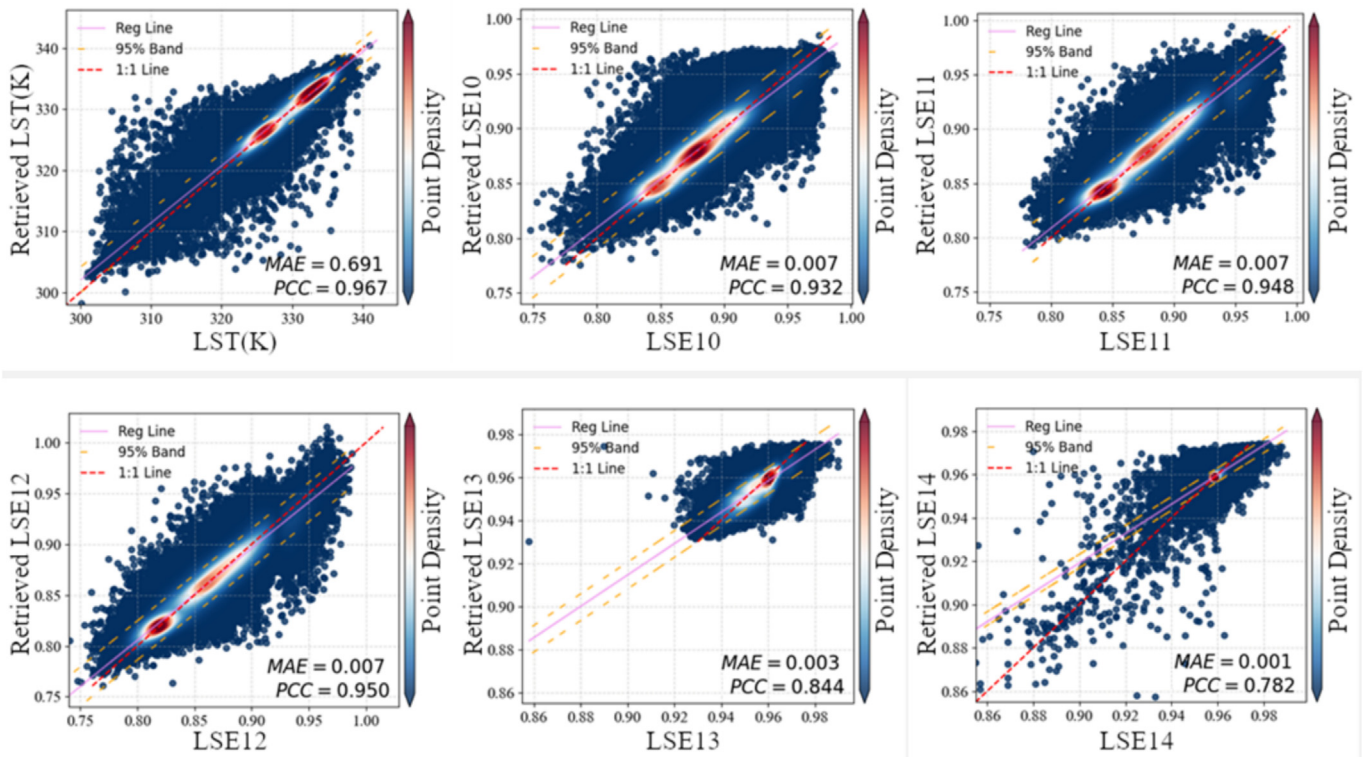


Fig. 3. Large model LST & LSE inversion scatter plot and accuracy display.

when facing data with limited precision. Therefore, it is necessary to use knowledge distillation technology, utilizing the large model as a teacher model to guide the small model through dataset distillation, ultimately forming an efficient student model to enhance and potentially match the large model's global inversion accuracy.

4.3. Application and analysis of knowledge distillation

As analyzed in Section 4.2, the small models exhibit limited accuracy due to constrained data. Despite the large model being trained with high-precision datasets, its application for inverting data from the

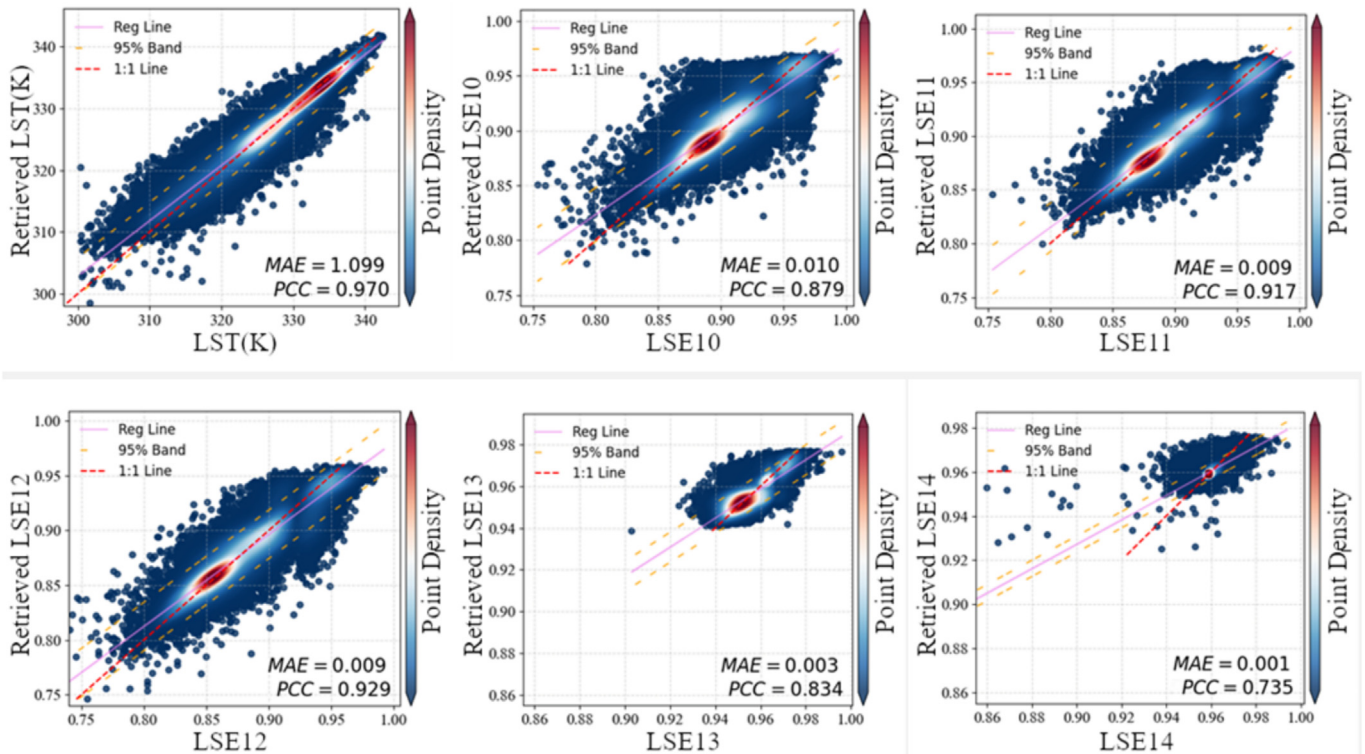


Fig. 4. Small model 1 LST & LSE inversion scatter plot and accuracy display.

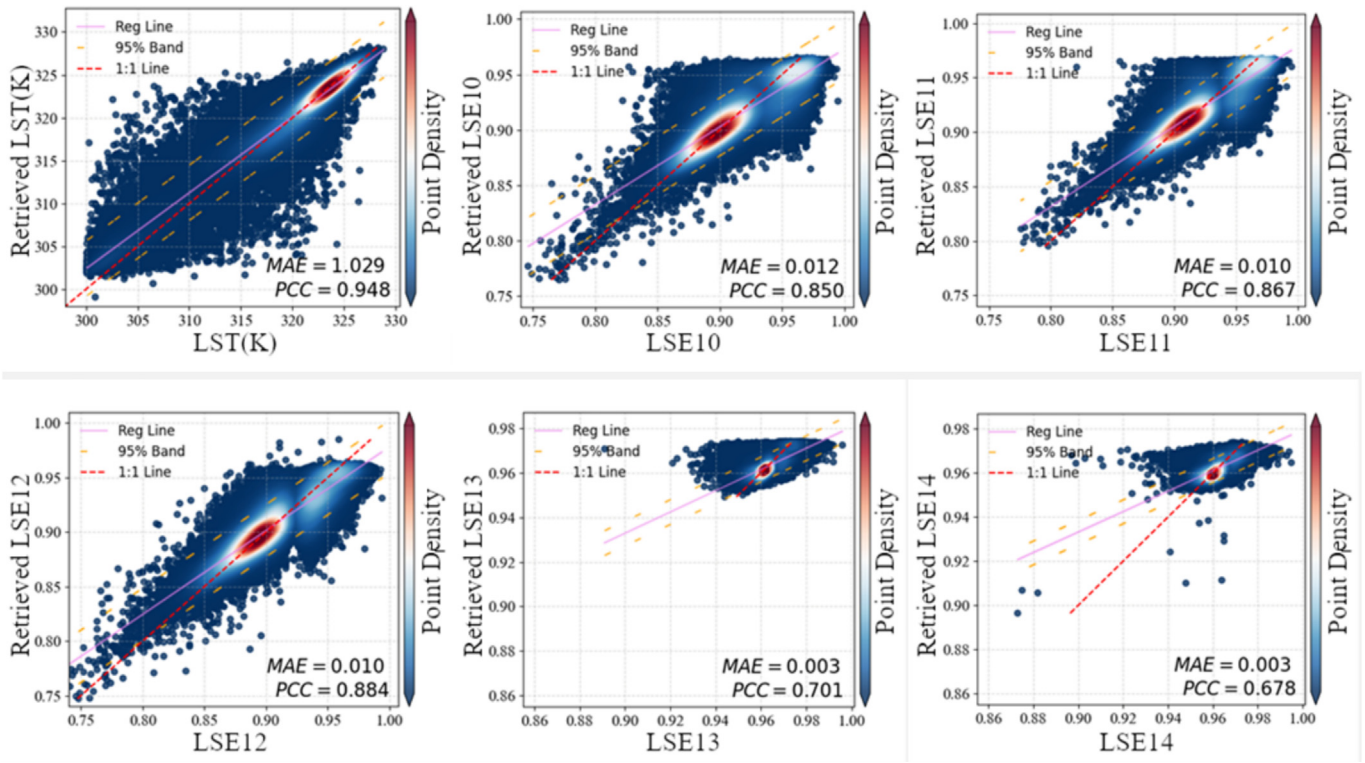


Fig. 5. Small model 2 LST & LSE inversion scatter plot and accuracy display.

small model datasets did not yield satisfactory accuracy. Therefore, it is necessary to employ knowledge distillation techniques to transfer knowledge from the large model to the small models, thereby optimizing the small models under the guidance of a high-precision model with generalizability.

4.3.1. Knowledge distillation weight design and analysis

To guide the formulation of an effective distillation strategy, this study adopted a rigorous statistical method—the independent sample *t*-test. This method aims to assess the statistical significance of performance improvements under different weight configurations. For this

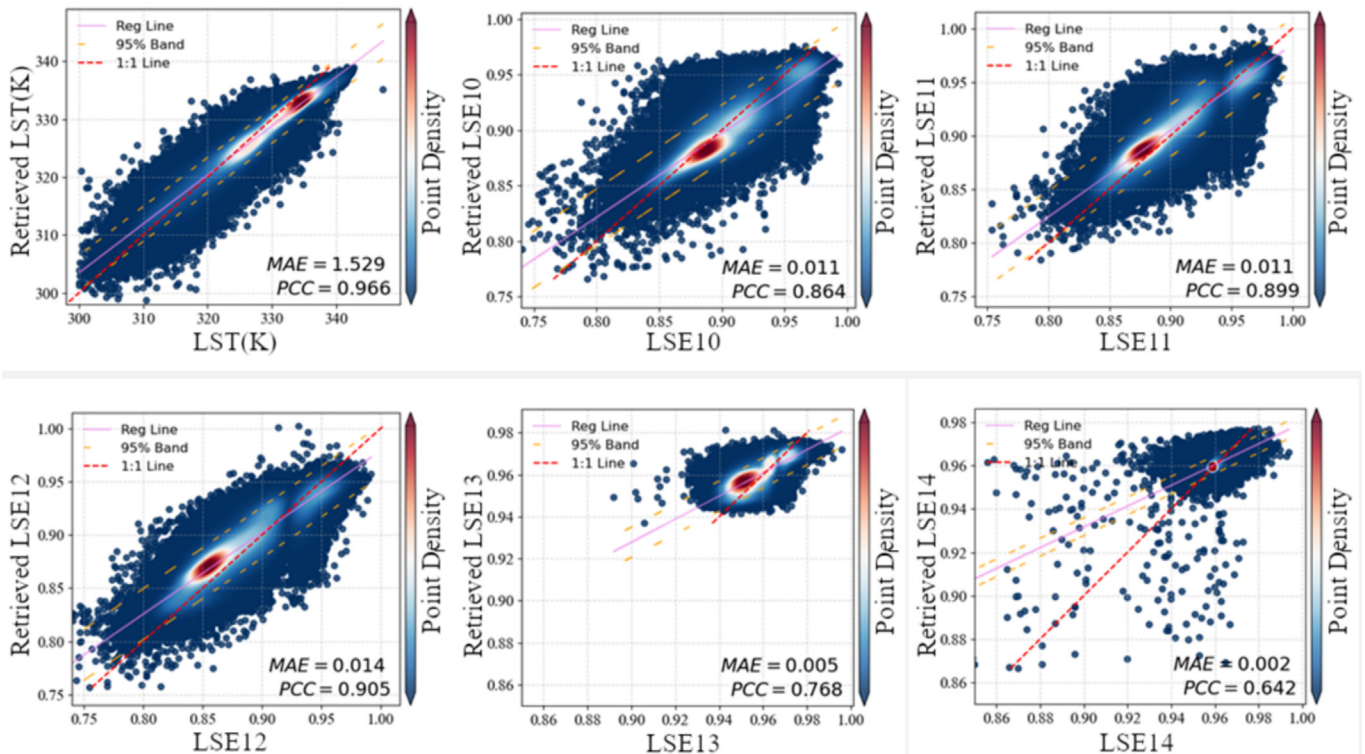


Fig. 6. Large model on small model 1 data LST & LSE inversion scatter plot and accuracy display.

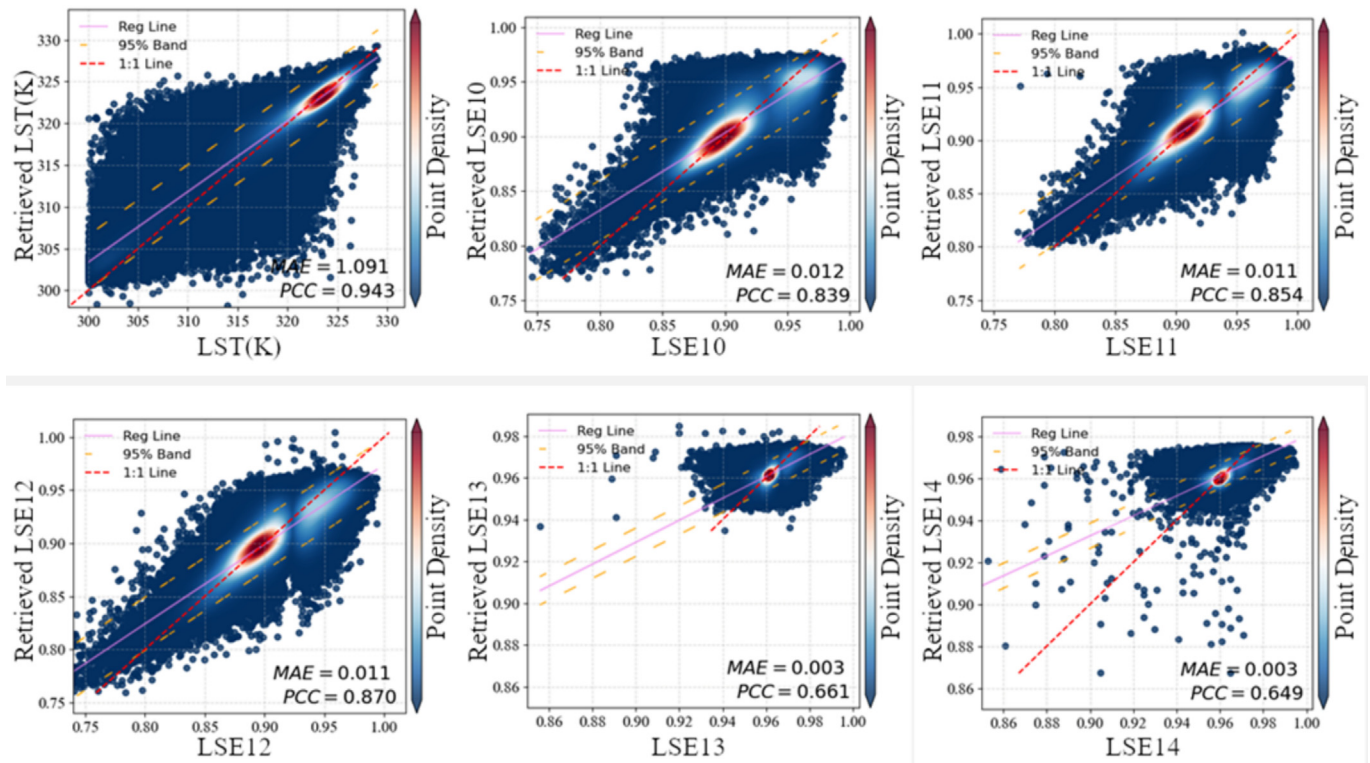


Fig. 7. Large model on small model 2 data LST & LSE inversion scatter plot and accuracy display.

purpose, 30 sets of knowledge distillation experiments were conducted without involving dataset distillation, thus collecting a series of data on model accuracy in its original state and after adjusting weights.

By meticulously applying the aforementioned statistical framework, this study conducted an in-depth analysis of data from 30 experiments under different weight configurations to evaluate the specific impact of weight adjustments on model performance. The following table (Table 4) summarizes the statistical analysis results of knowledge distillation for small model 1 surface temperature inversion, showing t-values and p-values calculated based on PCC and MAE for different weights.

By analyzing the t-statistics and p-values of PCC and MAE under different alphas, the relative changes in contributions from the teacher and student models can be observed. As alpha increases, the t-statistic gradually decreases, its absolute value first decreases then increases, indicating that as alpha increases, the student model's contribution diminishes, and the teacher model's contribution increases. All p-values under different alphas are significant, confirming the reliability of the statistical results.

Table 4
Statistical results of teacher and student contributions based on PCC and MAE under different weights.

Alpha	PCC		MAE	
	t-statistic	p-value	t-statistic	p-value
0.1	102.426	1.13E-38	66.68	2.73E-33
0.2	26.752	5.45E-22	4.674	6.28E-05
0.3	5.353	9.51E-06	-15.62	1.18E-15
0.4	-3.323	2.42E-03	-29.069	5.33E-23
0.5	-14.262	1.23E-14	-39.13	1.19E-26
0.6	-32.6	2.11E-24	-77.486	3.59E-35
0.7	-51.128	5.67E-30	-79.88	1.49E-35
0.8	-63.371	1.18E-32	-176.301	1.68E-45
0.9	-111.902	8.74E-40	-133.027	5.86E-42

To precisely define the optimal weight in the knowledge distillation process, 30 rounds of differentiated weight distillation experiments were carried out on six different inversion results of LST and LSE10 to LSE14 for small models 1 and 2. To further analyze the contribution of different weights to model accuracy enhancement, the evaluation function $f(t) = 1 / (\ln(|t| + e))$ was used to quantify the relative utility of weights through the statistical t and further normalize data to plot the corresponding radar chart (Fig. 8), where θ represents the weights at different dimensions, indicating the relative contributions of weights.

Analysis of the radar charts reveals the relative contributions of different inversion results at each weight to improvements in MAE and PCC indicators. Observations show that for improving MAE, the optimal weights for optimizing small models 1 and 2 are primarily concentrated at 0.2 and 0.3. For the PCC indicator, the best weights extend to 0.2, 0.3, and 0.4. As weights deviate from the optimum, their contribution to performance enhancement decreases; specifically, the further the deviation from the optimum, the weaker the positive impact on performance. Finally, box plots (Fig. 9) of different inversion results' optimal weights are drawn to further analyze the findings.

In the box plot analysis, the median for small model 1 is at 0.35, with the interquartile range spanning from 0.275 to 0.5. For small model 2, the median is at 0.3, with the interquartile range from 0.2 to 0.425. The interquartile range represents the central 50% clustering area of the data, providing a basis for assessing the data's central tendency and dispersion. With weight 0.3 occupying a central position in both models and also at the lower edge of the interquartile range in small model 1, the study identifies 0.3 as the optimal weight for enhancing small models in the knowledge distillation process, reflecting data's central tendency while maintaining consistency across models. This weight not only ensures that small models receive effective guidance from the teacher model but also maintains their own learning momentum as student models, achieving optimal knowledge distillation effects.

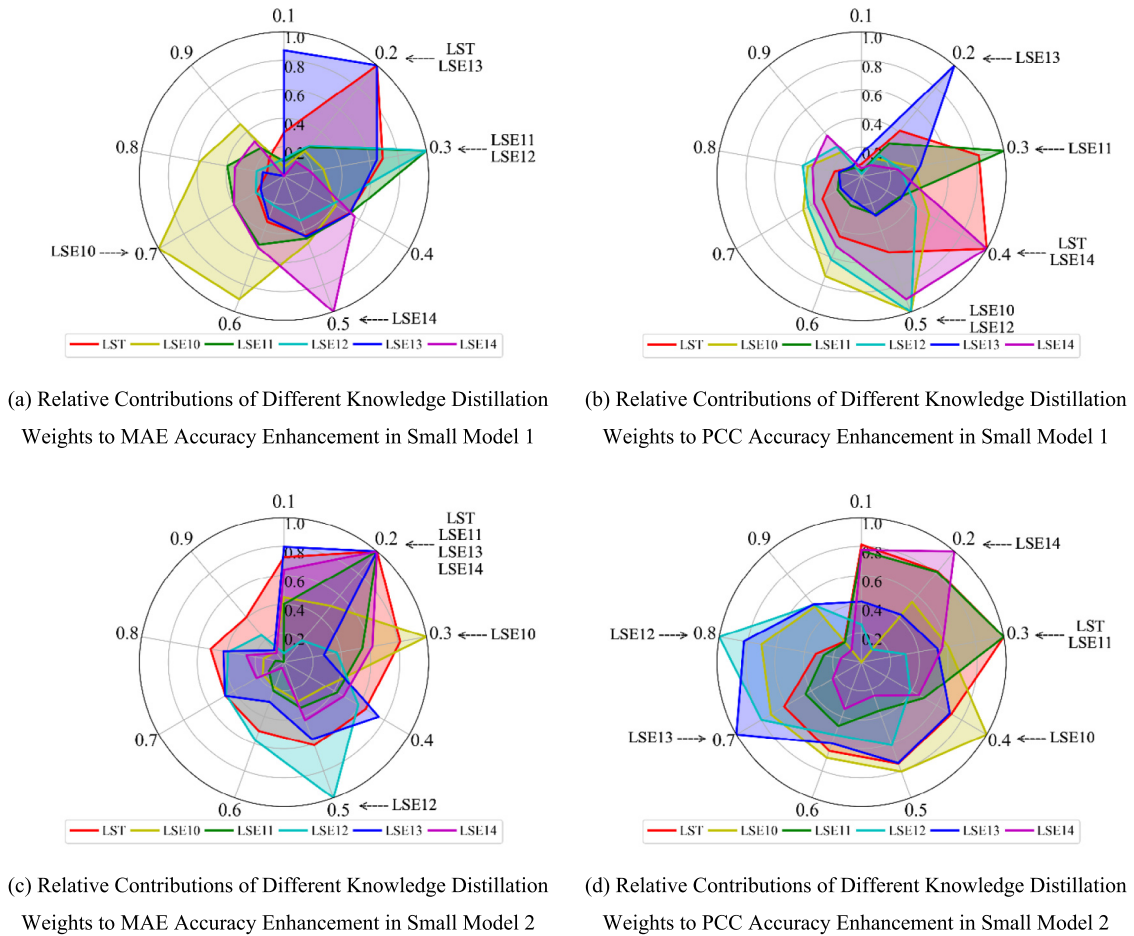


Fig. 8. Radar charts of relative contributions to model accuracy enhancement through knowledge distillation under different weights.

4.3.2. Student model optimization analysis

Based on prior statistical test analyses, a key distillation weight of 0.3 was selected to maintain precision enhancement while using the large model as the teacher model. This approach guided two small models through dataset distillation to reconstruct the inversion target dataset, bridging the gap between actual values and predictions, and producing an accurate approximation of real inversion target values, thus forming an efficient student model. Subsequently, scatter plots and accuracy displays of the optimized student models 1 and 2 after knowledge distillation are presented (Figs. 10 and 11).

A bar chart (Fig. 12) compares changes in various inversion indices before and after knowledge distillation.

Performance analysis of the optimized student models 1 and 2 shows notable improvements across all inversion indices. Specifically, in key LST bands, student model 1's PCC improved from 0.970 to 0.984; MAE decreased from 1.099 K to 0.731 K. Student model 2's

PCC increased from 0.948 to 0.973; MAE reduced from 1.029 K to 0.716 K. These results highlight the significant effects of knowledge distillation in enhancing model accuracy and reducing prediction errors. In emissivity bands LSE10 to LSE14, both improved models also showed significant performance enhancements, with student model 1's average PCC increasing from 0.859 to 0.917, and average MAE decreasing from 0.0064 to 0.0044. Student model 2's average PCC improved from 0.796 to 0.879, and average MAE reduced from 0.0088 to 0.0064. The Taylor diagram for model accuracy improvement is shown in Fig. 13, with a zoom in on the overlapping data points in the figure.

In Fig. 13, the model inversion results have been standardized such that the observation data point (Observed Values, OBS) maintains a standard deviation (SD) of 1, enabling normalized comparison of model performance against ground truth. In this representation, the distance between a scatter point and the OBS reference on the x-axis quantifies the root mean square error (RMSE) - closer proximity to the OBS point indicates higher model accuracy. The radial distance from the origin represents SD, while the angular coordinate corresponds to the Pearson correlation coefficient (PCC) indicated by the graduated arcs. The diagram illustrates: LMI (Large Model Inversion) accuracy; SMI_1 and SMI_2 representing Small Model Inversion variants; LMIS_1 and LMIS_2 denoting large model performance when processing small model datasets; and KSMI_1/KSMI_2 showing knowledge-distilled small model capabilities. Although the large model demonstrates superior PCC compared to baseline small models, its compromised RMSE performance in cross-model inversion scenarios reveals inherent data compatibility limitations. Conversely, knowledge-distilled small models exhibit optimized balance - achieving comparable PCC while

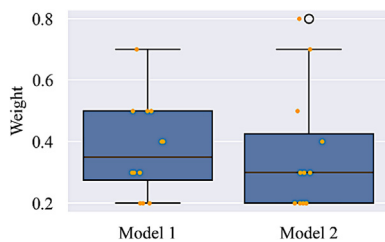


Fig. 9. Box plots of optimal weights for different inversion results.

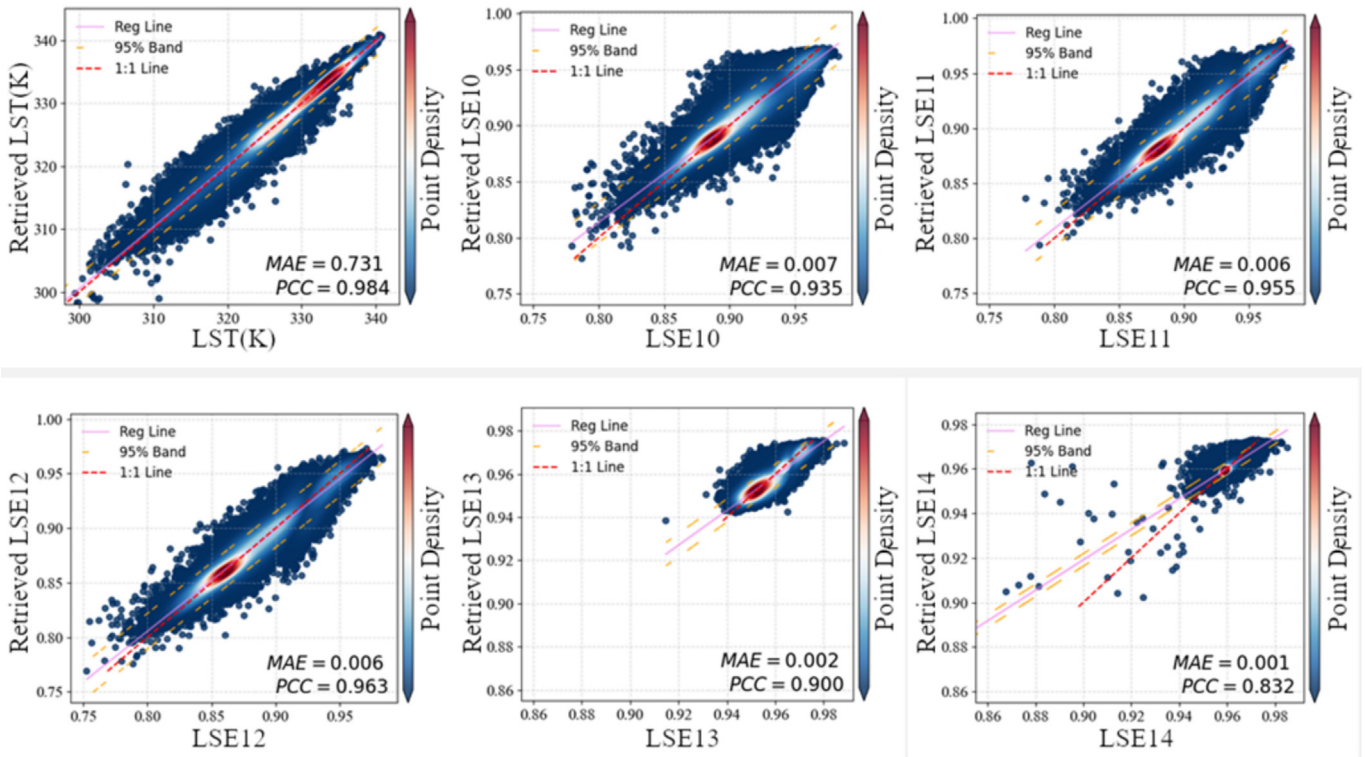


Fig. 10. Student model 1 LST & LSE inversion scatter plot and accuracy display.

demonstrating RMSE metrics that approach or occasionally surpass those of the large model architecture.

The analysis demonstrates that the knowledge distillation strategy effectively enhanced the precision of small models in surface temperature and emissivity inversion, particularly showing substantial potential

when dealing with complex data and limited resources. This provides important support for enhancing the robustness and reliability of models in practical applications. The optimized student models were then integrated interactively into the large model to form a high-quality jointly optimized model. In the joint optimization model,

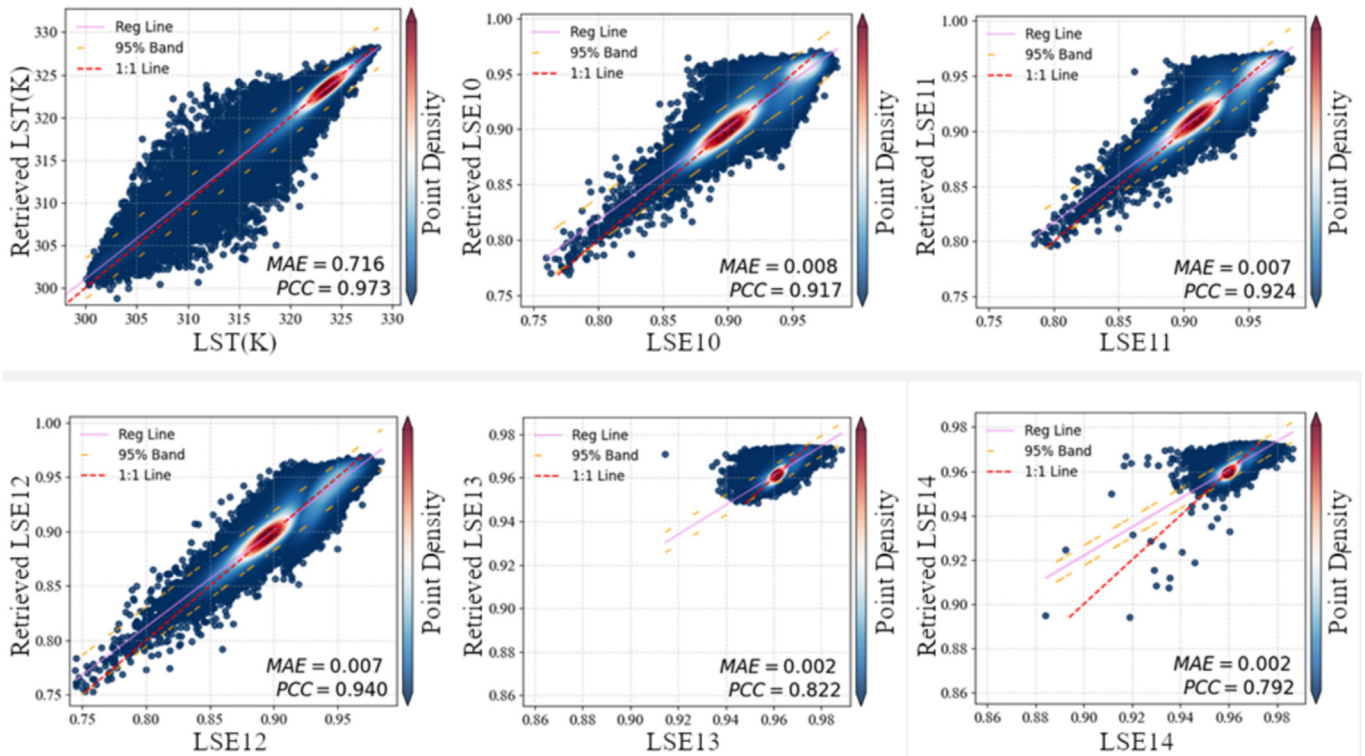


Fig. 11. Student model 2 LST & LSE inversion scatter plot and accuracy display.

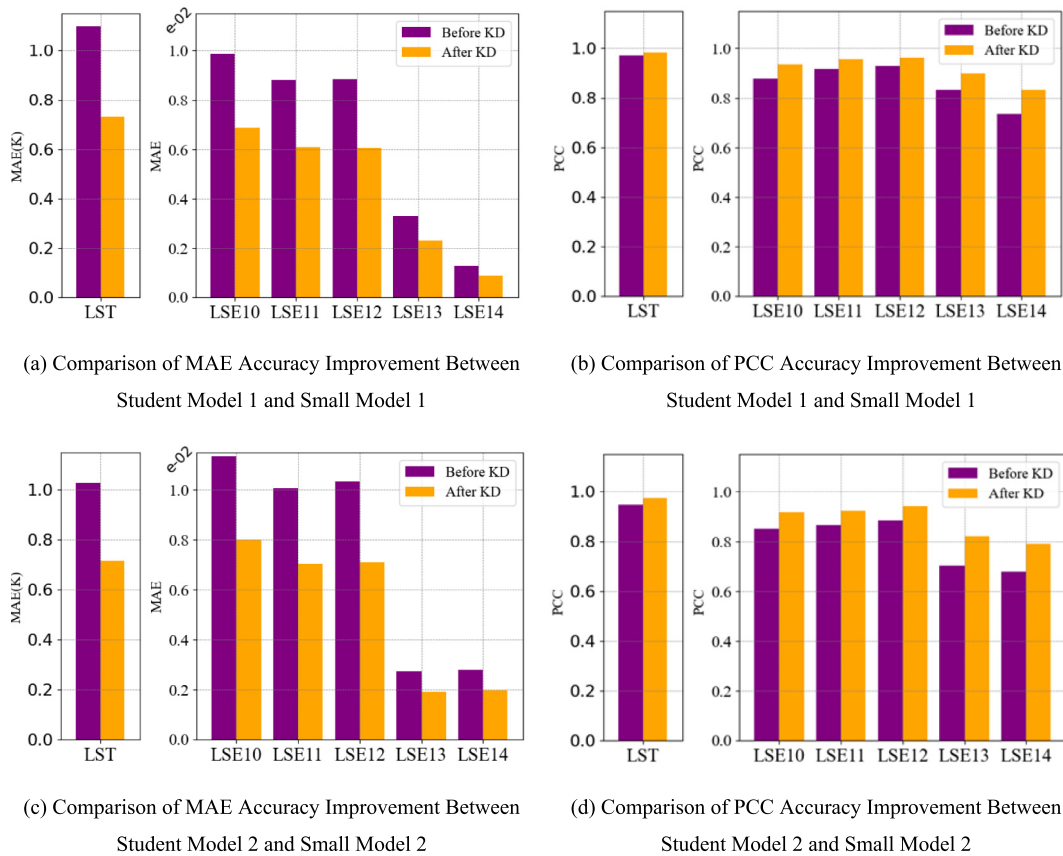


Fig. 12. Bar chart comparing inversion accuracy before and after knowledge distillation.

models adapted to the data's source regions were selected, further enhancing the model's specificity and generalization capability.

4.4. Cross-validation and ground validation

4.4.1. Cross-validation

Cross-validation is valuable in identifying spatial differences between products and inversion values, especially considering variations in spatial resolution and temporal sequences across different satellite datasets. Compared to emissivity, surface temperature data is more representative. This study selected MODIS surface temperature datasets corresponding to two small model areas for detailed cross-validation of the small models and their optimized student models. The analysis included four sets of comparative images (Figs. 14 and 15), covering surface temperature maps, model prediction scatter plots, and prediction error distribution maps to comprehensively assess model performance.

Cross-validation revealed that student model 1's surface temperature inversion MAE decreased from 2.416 K to 1.730 K and PCC increased from 0.832 to 0.912 after knowledge distillation; student model 2's LST inversion MAE decreased from 2.345 K to 1.666 K and PCC improved from 0.777 to 0.893, demonstrating the effectiveness of the knowledge distillation optimization strategy in enhancing prediction accuracy. Detailed observation of the error distribution maps showed a reduction in error range and a significant increase in zero-error frequency, indicating a marked enhancement in the consistency between model predictions and actual observations.

Additionally, by comparing MODIS temperature distribution maps with predicted temperature distribution maps, the optimized models not only aligned overall with MODIS surface temperature distributions but also displayed richer detail features using ASTER's high resolution. This analysis highlights the practical value of the knowledge distillation

strategy in finely tuning surface temperature inversion models to convey teacher knowledge.

4.4.2. Ground data validation

Compared to emissivity, surface temperature data from ground is more readily available. Therefore, this study primarily focuses on validating the effectiveness of our proposed method by comparing satellite-inferred surface temperatures with ground measurement data. The accuracy of ground-based measurements directly impacts data collection, and to eliminate interference through strict quality control, the study selected representative and highly precise clear-sky, flat terrain measurement data. Considering the complexity of ground validation, robust statistics required an appropriate outlier removal strategy. For this purpose, we adopted the new 3-sigma criterion proposed (Sobrino et al., 2016), which is based on theoretical uncertainties related to the algorithm. Specifically, outliers were removed using a threshold of three times the theoretical precision to eliminate anomalies between the inverted and ground-measured surface temperatures. Subsequent ground validations were conducted for small models 1 and 2, and student models 1 and 2, with their scatter plots and accuracy displays shown in Fig. 16.

Optimization through the knowledge distillation strategy significantly enhanced the performance of student model 1 in ground data validation, with its Pearson Correlation Coefficient (PCC) increasing from 0.963 to 0.986 and Mean Absolute Error (MAE) decreasing from 1.953 K to 1.315 K. Similarly, student model 2 showed improvements post-optimization, with its PCC rising from 0.940 to 0.970 and MAE reducing from 1.988 K to 1.414 K. Although the accuracy in ground data validation was slightly lower than the validation results based on ASTER satellite data, considering the real physical conditions represented by the ground data, such as local terrain variations, vegetation cover, and the thermal properties of ground materials, the results of

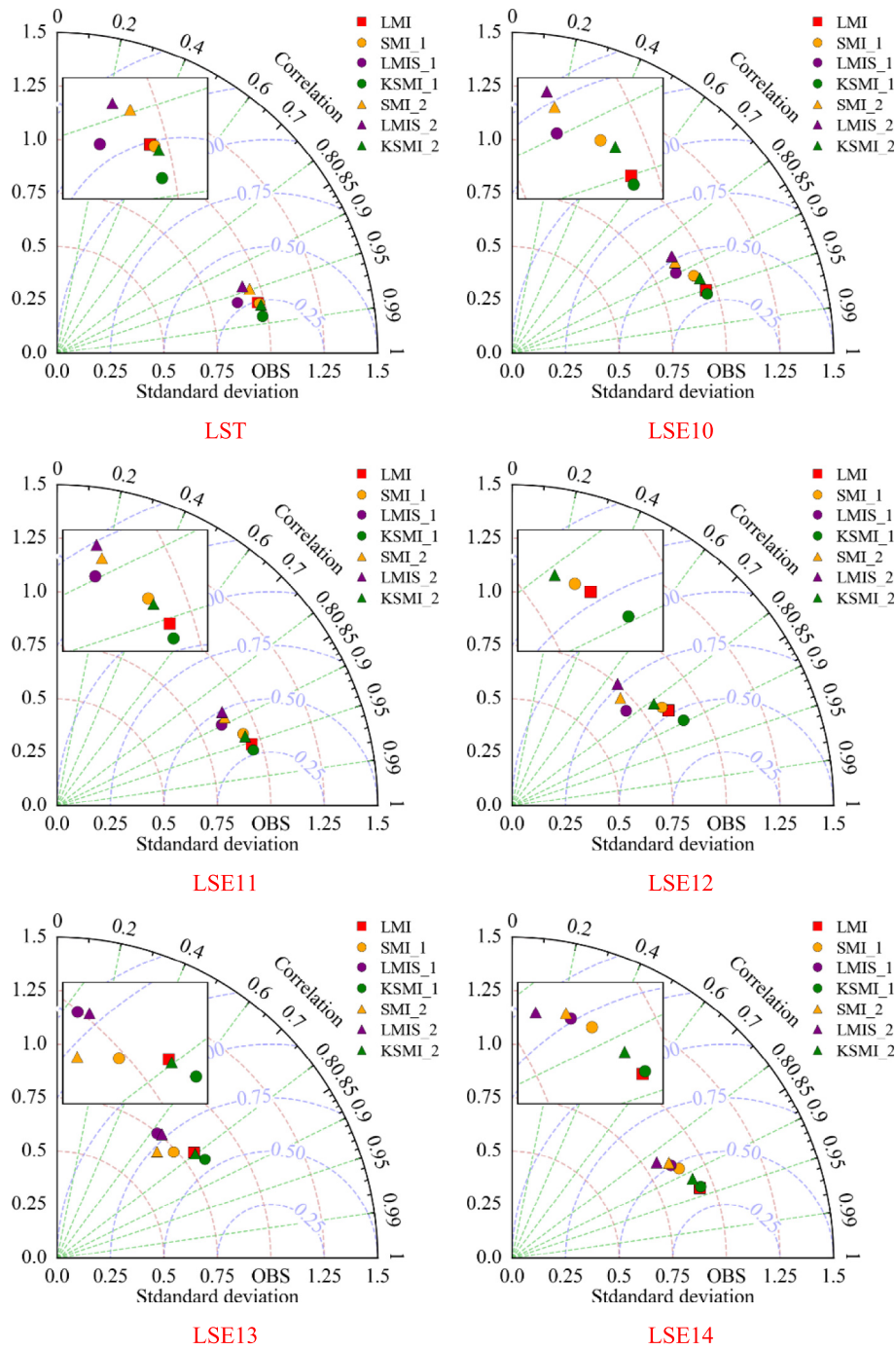


Fig. 13. Taylor diagram for model accuracy comparison.

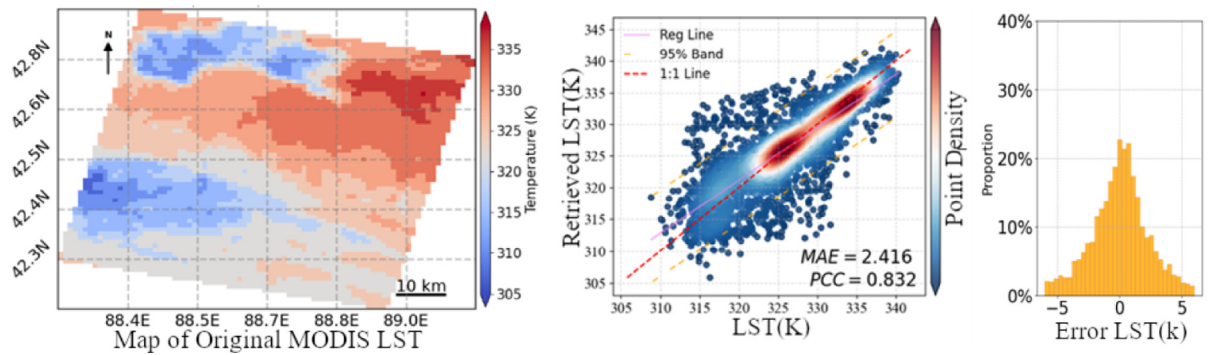
ground validation to some extent confirm the reliability and practical value of our proposed method. This further substantiates the robustness and efficacy of the knowledge distillation strategy when facing complex real-world physical conditions.

5. Conclusion and future prospects

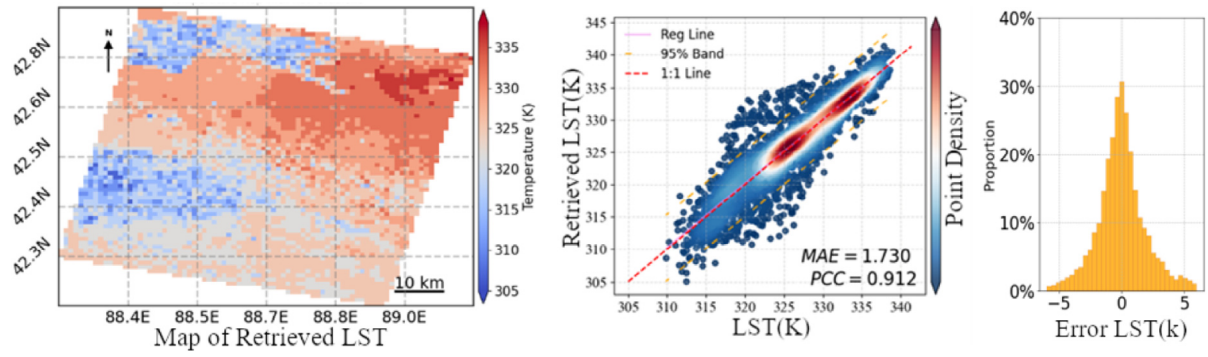
This study aimed to address the challenges posed by the complexity and nonlinear characteristics of Earth systems on the accuracy of local model inversion. By integrating cutting-edge artificial intelligence technologies—automated machine learning, large-scale models, and knowledge distillation—we significantly enhanced the local inversion performance of thermal infrared remote sensing parameters (LST &

LSE) and developed a jointly optimized model for precise global remote sensing parameter inversion.

Theoretical analyses confirmed the applicability of knowledge distillation in remote sensing parameter inversion. Combining physical and statistical methods, we elucidated the fundamental principles of deep learning in model training and explored the effectiveness of automated network architecture and hyperparameter configuration using AutoKeras. These findings provided a solid theoretical foundation for the AK-KD strategy, enhanced the physical interpretability of the model, and significantly improved remote sensing inversion accuracy. A large model trained using ASTER simulated data (selecting bands 10 to 14, with an LST step size of 1) exhibited excellent performance in surface temperature inversion, achieving a Pearson Correlation Coefficient

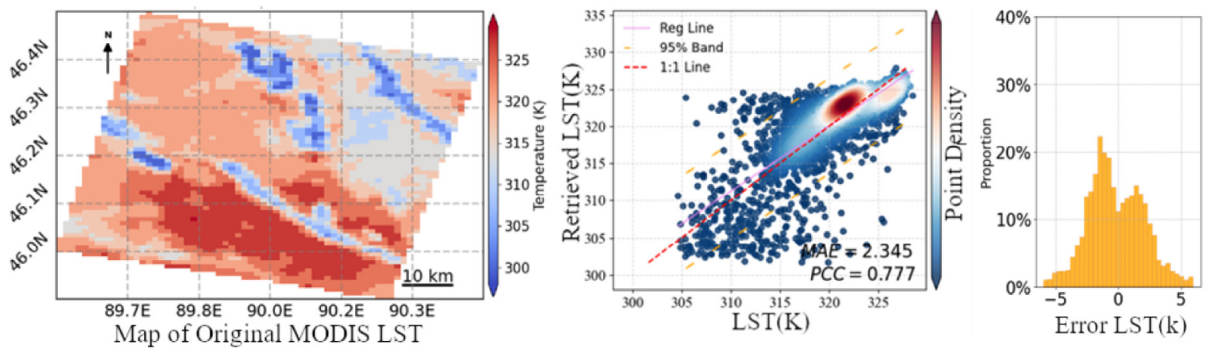


(a) Inversion Results for Small Model 1

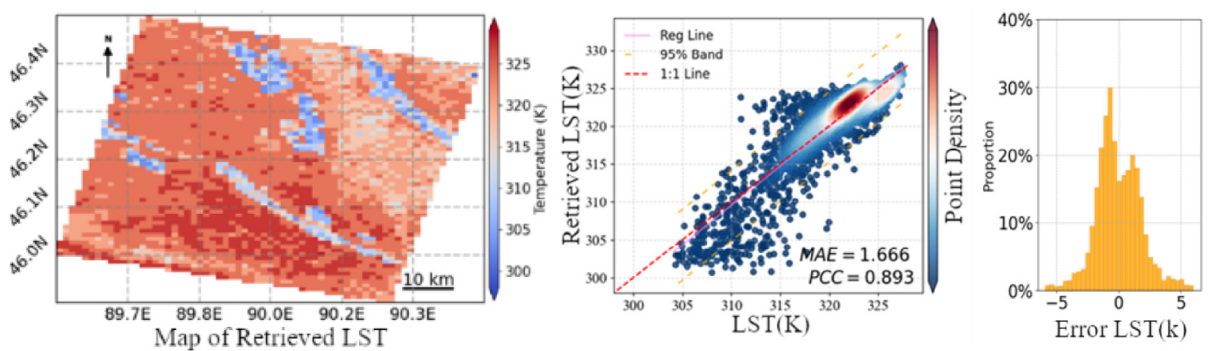


(b) Inversion Results for Student Model 1

Fig. 14. Model 1 surface temperature map, cross-validation scatter plot, prediction error distribution map.

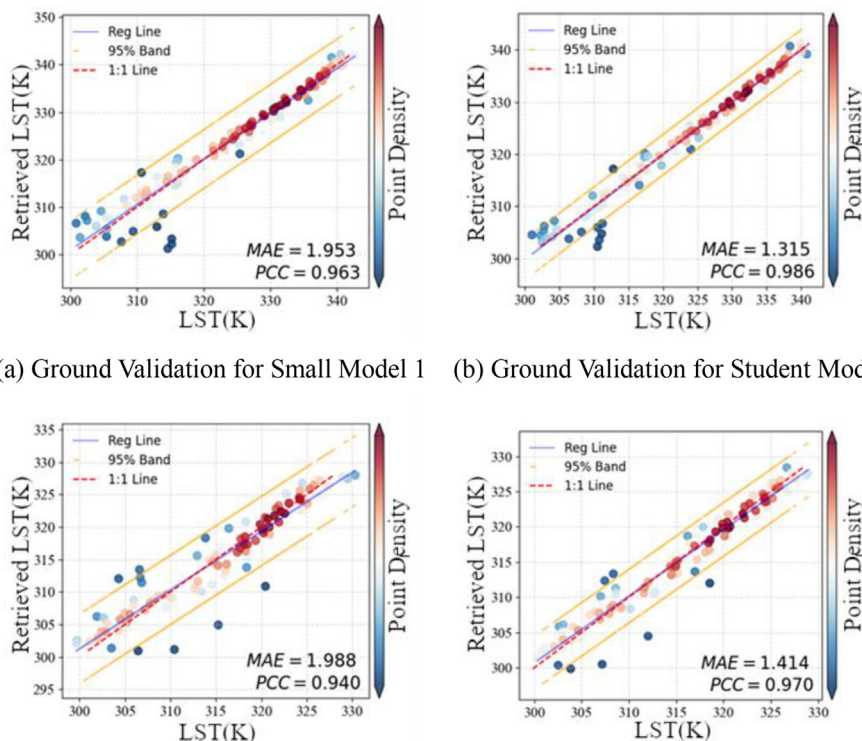


(c) Inversion Results for Small Model 2



(d) Inversion Results for Student Model 2

Fig. 15. Model 2 surface temperature map, cross-validation scatter plot, prediction error distribution map.



(a) Ground Validation for Small Model 1 (b) Ground Validation for Student Model 1
(c) Ground Validation for Small Model 2 (d) Ground Validation for Student Model 2

Fig. 16. Ground validation scatter plots.

(PCC) of 0.999 and a Mean Absolute Error (MAE) of 0.348 K. In practical applications, this model achieved a PCC of 0.967 and MAE of 0.685 K in surface temperature inversion. By using this large model as a teacher model to optimize small models, the inversion accuracy for LST and bands LSE10 to LSE14 was significantly enhanced. Specifically, in surface temperature inversion, the small model's average PCC increased from 0.978 to 0.979; average MAE decreased from 1.065 K to 0.724 K. In emissivity inversion, the average PCC rose from 0.827 to 0.898; average MAE reduced from 0.0076 to 0.0054. Cross-validation and ground validation results reinforced the reliability of these outcomes and demonstrated the potential of knowledge distillation technology in enhancing local inversion accuracy.

In future research endeavors, we intend to amalgamate large and small model architectures trained on both high and low-resolution data, employing knowledge distillation techniques to engender lightweight student models that embody both extensive coverage and refined inversion capabilities. Furthermore, we aim to further integrate intelligence optimization with interactive dynamic fusion technology (Balasubramani and Natarajan, 2024), in conjunction with the temporal attention mechanism to capture the nonlinear dynamic characteristics of multi-temporal remote sensing data, thereby training a large teacher model. Concurrently, we will construct an adaptive joint optimization model based on data sources and regional characteristics. The integration of such technologies holds the promise of enhancing the model's adaptability to environmental complexities and propelling the inversion of remote sensing parameters towards greater intelligence and cross-scenario versatility.

CRedit authorship contribution statement

Wang Dai: Writing – review & editing, Writing – original draft, Visualization, Validation, Supervision, Software, Resources, Project administration, Methodology, Investigation, Formal analysis, Data curation, Conceptualization. **Kebiao Mao:** Writing – review & editing, Writing –

original draft, Supervision, Resources, Project administration, Methodology, Funding acquisition, Formal analysis, Conceptualization. **Zhonghua Guo:** Writing – review & editing, Validation, Formal analysis. **Zhihao Qin:** Writing – review & editing, Supervision. **Jiancheng Shi:** Writing – review & editing, Supervision. **Sayed M. Bateni:** Writing – review & editing, Supervision. **Liurui Xiao:** Writing – review & editing, Supervision.

Declaration of competing interest

The authors declare that they have no known competing financial interests or personal relationships that could have appeared to influence the work reported in this paper.

Acknowledgments

We are especially thankful to NASA and Japan's Ministry of Economy, Trade and Industry (METI) for providing the ASTER thermal infrared data that were crucial for our analysis. Additionally, we are thankful to the Chinese Academy of Sciences, Institute of Geographic Sciences and Natural Resources Research for providing ground observation data. This research was supported by the Key Project of Natural Science Foundation of Ningxia Department of Science and Technology (No. 2024AC02032), Fengyun Satellite Application Pilot Program Central Public-interest Scientific Institution Basal Research Fund (No. Y2025YC86), Development and Application of Fengyun all-weather Land Surface Temperature Spatiotemporal Fusion Dataset (FY-APP-2022.0205), Central Public-interest Scientific Institution Basal Research Fund (No. Y2025YC86).

References

- Ananthaswamy, A., 2023. In AI, is bigger always better? *Nature* 615 (7951), 202–205.
- Bagherinezhad, H., Horton, M., Rastegari, M., Farhadi, A., 2018. Label Refinery: Improving Imagenet Classification Through Label Progression. *arXiv preprint*, pp. 1–16 arXiv: 1805.02641.

- Balasubramani, K., Natarajan, U.M., 2024. Improving bus passenger flow prediction using Bi-LSTM fusion model and SMO algorithm. *Babylonian J. Artif. Intell.* 2024, 73–82.
- Bubeck, S., Sellke, M., 2023. A universal law of robustness via isoperimetry. *J. ACM* 70 (2), 1–18.
- Cao, M., Mao, K., Bateni, S.M., Jun, C., Shi, J., Du, Y., Du, G., 2023. Granulation-based lstm-f combination model for hourly sea surface temperature prediction. *Int. J. Digit. Earth* 16 (1), 3838–3859.
- Carter, C., Liang, S., 2019. Evaluation of ten machine learning methods for estimating terrestrial evapotranspiration from remote sensing. *Int. J. Appl. Earth Obs. Geoinf.* 78, 86–92.
- Duan, S.B., Han, X.J., Huang, C., Li, Z.L., Wu, H., Qian, Y., Gao, M., Leng, P., 2020. Land surface temperature retrieval from passive microwave satellite observations: state-of-the-art and future directions. *Remote Sens.* 12 (16), 1–27.
- Frey, C.M., Kuenzer, C., Dech, S., 2017. Assessment of mono-and split-window approaches for time series processing of LST from AVHRR-A TIMELINE round robin. *Remote Sens.* 9 (1), 1–24.
- Furlanello, T., Lipton, Z., Tschannen, M., Itti, L., Anandkumar, A., 2018. Born again neural networks. *International Conference on Machine Learning*. PMLR, pp. 1607–1616.
- Gou, J., Yu, B., Maybank, S.J., Tao, D., 2021. Knowledge distillation: a survey. *Int. J. Comput. Vis.* 129 (6), 1789–1819.
- He, X., Zhao, K., Chu, X., 2021. AutoML: a survey of the state-of-the-art. *Knowl.-Based Syst.* 212, 1–27.
- Hinton, G., Vinyals, O., Dean, J., 2015. Distilling the Knowledge in a Neural Network. *arXiv preprint*, pp. 1–9 arXiv:1503.02531.
- Jia, H., Yang, D., Deng, W., Wei, Q., Jiang, W., 2021. Predicting land surface temperature with geographically weighed regression and deep learning. *Wiley Interdiscip. Rev. Data Min. Knowl. Discov.* 11 (1), 1–19.
- Jin, H., Song, Q., Hu, X., 2019. Auto-keras: an efficient neural architecture search system. *Proceedings of the 25th ACM SIGKDD International Conference on Knowledge Discovery Data Mining*, pp. 1946–1956.
- Jin, H., Chollet, F., Song, Q., Hu, X., 2023. Autokeras: an automl library for deep learning. *J. Mach. Learn. Res.* 24 (6), 1–6.
- Joshi, C., De Leeuw, J., Skidmore, A.K., Van Duren, I.C., Van Oosten, H., 2006. Remotely sensed estimation of forest canopy density: a comparison of the performance of four methods. *Int. J. Appl. Earth Obs. Geoinf.* 8 (2), 84–95.
- Kelenyi, B., Domsa, V., Tamas, L., 2024. SAM-Net: self-attention based feature matching with spatial transformers and knowledge distillation. *Expert Syst. Appl.* 242, 1–12.
- Li, J., Hong, D., Gao, L., Yao, J., Zheng, K., Zhang, B., Chanussot, J., 2022. Deep learning in multimodal remote sensing data fusion: a comprehensive review. *Int. J. Appl. Earth Obs. Geoinf.* 112, 1–16.
- Li, J., Guan, Y., Lu, Q., Bao, Y., Wu, C., Xu, C., 2023a. Retrieval of desert microwave land surface emissivity based on machine learning algorithms. *Remote Sens.* 16 (1), 1–19.
- Li, K., Song, J., Xia, S., Luo, B., Wang, J., Zhong, Y., Ren, S., 2023b. Salt structure identification based on U-net model with target flip, multiple distillation and self-distillation methods. *Front. Earth Sci.* 10, 1–21.
- Lin, Y.K., Wang, C.F., Chang, C.Y., Sun, H.L., 2021. An efficient framework for counting pedestrians crossing a line using low-cost devices: the benefits of distilling the knowledge in a neural network. *Multimed. Tools Appl.* 80, 4037–4051.
- Luo, Y., Yin, L., Bai, W., Mao, K., 2020. An appraisal of incremental learning methods. *Entropy* 22 (11), 1–27.
- Mao, K., Shi, J., Li, Z., Tang, H., 2007. An RM-NN algorithm for retrieving land surface temperature and emissivity from EOS/MODIS data. *J. Geophys. Res.* 112 (D21102), 1–17.
- Mao, K., Shi, J., Tang, H., Li, Z.L., Wang, X., Chen, K.S., 2008. A neural network technique for separating land surface emissivity and temperature from ASTER imagery. *IEEE Trans. Geosci. Remote Sens.* 46 (1), 200–208.
- Mao, K., Li, S., Wang, D., Zhang, L., Wang, X., Tang, H., Li, Z.L., 2011. Retrieval of land surface temperature and emissivity from ASTER1B data using a dynamic learning neural network. *Int. J. Remote Sens.* 32 (19), 5413–5423.
- Mao, K., Wang, H., Shi, J., Heggy, E., Wu, S., Bateni, S.M., Du, G., 2023. A general paradigm for retrieving soil moisture and surface temperature from passive microwave remote sensing data based on artificial intelligence. *Remote Sens.* 15 (7), 1–20.
- Mao, K., Wu, C., Yuan, Z., Liu, Y., Cao, M., Wang, H., 2024. Theory and conditions for AI-based inversion paradigm of geophysical parameters using energy balance. *EarthArXiv* 12, 1–26. <https://doi.org/10.31223/X5H13J>.
- Mas, J.F., Flores, J.J., 2008. The application of artificial neural networks to the analysis of remotely sensed data. *Int. J. Remote Sens.* 29 (3), 617–663.
- Mei, R., Mao, K., Shi, J., Nielson, J., Bateni, S.M., Meng, F., Du, G., 2023. A novel physics-statistical coupled paradigm for retrieving integrated water vapor content based on artificial intelligence. *Remote Sens.* 15 (17), 1–22.
- Mittal, S., Galesso, S., Brox, T., 2021. Essentials for class incremental learning. *Proceedings of the IEEE/CVF Conference on Computer Vision and Pattern Recognition*, pp. 3513–3522.
- Moisa, M.B., Gabissa, B.T., Hinkosa, L.B., Dejene, I.N., Gemedo, D.O., 2022. Analysis of land surface temperature using geospatial technologies in Gida Kiremu, Limu, and Amuru District, Western Ethiopia. *Artif. Intell. Agric.* 6, 90–99.
- Naveed, H., Khan, A.U., Qiu, S., Saqib, M., Anwar, S., Usman, M., Akhtar, N., Barnes, N., Mian, A., 2023. A Comprehensive Overview of Large Language Models. *arXiv preprint*, pp. 1–34 arxiv:2307.06435.
- Phuong, M., Lampert, C., 2019. Towards understanding knowledge distillation. *International Conference on Machine Learning*. PMLR, pp. 5142–5151.
- Sobrinho, J.A., Jiménez-Muñoz, J.C., Sòria, G., Ruescas, A.B., Danne, O., Brockmann, C., Ghent, D., Remedios, J., North, P., Merchant, C., Berger, M., Mathieu, P.P., Göttsche, F.M., 2016. Synergistic use of MERIS and AATSR as a proxy for estimating land surface temperature from Sentinel-3 data. *Remote Sens. Environ.* 179, 149–161.
- Tan, J., NourEldeen, N., Mao, K., Shi, J., Li, Z., Xu, T., Yuan, Z., 2019. Deep learning convolutional neural network for the retrieval of land surface temperature from AMSR2 data in China. *Sensors* 19 (13), 1–20.
- Tang, J., Chen, S., Niu, G., Sugiyama, M., Gong, C., 2023. Distribution shift matters for knowledge distillation with webly collected images. *Proceedings of the IEEE/CVF International Conference on Computer Vision*, pp. 17470–17480.
- Tang, J., Chen, S., Niu, G., Zhu, H., Zhou, J.T., Gong, C., Sugiyama, M., 2024. Direct Distillation between Different Domains. *arXiv preprint*, pp. 1–11 arXiv:2401.06826.
- Wang, L., Yoon, K.J., 2021. Knowledge distillation and student-teacher learning for visual intelligence: a review and new outlooks. *IEEE Trans. Pattern Anal. Mach. Intell.* 44 (6), 3048–3068.
- Wang, S., He, L., Hu, W., 2015. A temperature and emissivity separation algorithm for landsat-8 thermal infrared sensor data. *Remote Sens.* 7 (8), 9904–9927.
- Wang, Y., Liu, D., Xie, W., Yang, M., Gao, Z., Ling, X., Huang, Y., Li, C., Liu, Y., Xia, Y., 2021a. Day and night clouds detection using a thermal-infrared all-sky-view camera. *Remote Sens.* 13 (9), 1–17.
- Wang, H., Mao, K., Yuan, Z., Shi, J., Cao, M., Qin, Z., Duan, S., Tang, B., 2021b. A method for land surface temperature retrieval based on model-data-knowledge-driven and deep learning. *Remote Sens. Environ.* 265, 1–19.
- Wang, H., Mao, K., Shi, J., Bateni, S.M., Altantuya, D., Sainbuyan, B., Bao, Y., 2024. A normal form for synchronous land surface temperature and emissivity retrieval using deep learning coupled physical and statistical methods. *Int. J. Appl. Earth Obs. Geoinf.* 127, 1–18.
- Wu, P., Yin, Z., Yang, H., Wu, Y., Ma, X., 2019. Reconstructing geostationary satellite land surface temperature imagery based on a multiscale feature connected convolutional neural network. *Remote Sens.* 11 (3), 1–18.
- Yang, G., Pu, R., Huang, W., Wang, J., Zhao, C., 2009. A novel method to estimate subpixel temperature by fusing solar-reflective and thermal-infrared remote-sensing data with an artificial neural network. *IEEE Trans. Geosci. Remote Sens.* 48 (4), 2170–2178.
- Yu, X., Guo, X., Wu, Z., 2014. Land surface temperature retrieval from Landsat 8 TIRS—comparison between radiative transfer equation-based method, split window algorithm and single channel method. *Remote Sens.* 6 (10), 9829–9852.
- Yuan, Q., Shen, H., Li, T., Li, Z., Li, S., Jiang, Y., Xu, H., Tan, W., Yang, Q., Wang, J., Gao, J., Zhang, L., 2020. Deep learning in environmental remote sensing: achievements and challenges. *Remote Sens. Environ.* 241, 1–24.
- Zhang, B., Zhang, M., Hong, D., 2021. Land surface temperature retrieval from Landsat 8 OLI/TIRS images based on back-propagation neural network. *Indoor Built Environ.* 30 (1), 22–38.